Loss of gastrokine-2 drives premalignant gastric inflammation and tumor progression

Trevelyan R. Menheniott,[1,2] Louise O'Connor,[1] Yok Teng Chionh,[1] Jan Däbritz,[1,2] Michelle Scurr,[1] Benjamin N. Rollo,[1] Garrett Z. Ng,[1] Shelley Jacobs,[1] Angelique Catubig,[1] Bayzar Kurklu,[1] Stephen Mercer,[1] Toshinari Minamoto,[3] David E. Ong,[4] Richard L. Ferrero,[5] James G. Fox,[6] Timothy C. Wang,[7] Philip Sutton,[1,8] Louise M. Judd,[1,2] and Andrew S. Giraud[1,2]

[1]Murdoch Children's Research Institute, Melbourne, Victoria, Australia. [2]Department of Paediatrics, University of Melbourne, Melbourne, Victoria, Australia. [3]Division of Translational and Clinical Oncology, Cancer Research Institute, Kanazawa University, Kanazawa, Japan. [4]University Medicine Cluster, Division of Gastroenterology and Hepatology, National University Hospital Singapore, Singapore. [5]Centre for Innate Immunity and Infectious Diseases, Monash Institute of Medical Research, Monash University, Clayton, Victoria, Australia. [6]Division of Comparative Medicine, Department of Biological Engineering, Massachusetts Institute of Technology, Cambridge, Massachusetts, USA. [7]Division of Digestive and Liver Disease, Department of Medicine, Columbia University Medical Center, New York, New York, USA. [8]Centre for Animal Biotechnology, School of Veterinary and Agricultural Science, University of Melbourne, Parkville, Victoria, Australia.

Chronic mucosal inflammation is associated with a greater risk of gastric cancer (GC) and, therefore, requires tight control by suppressive counter mechanisms. Gastrokine-2 (GKN2) belongs to a family of secreted proteins expressed within normal gastric mucosal cells. GKN2 expression is frequently lost during GC progression, suggesting an inhibitory role; however, a causal link remains unsubstantiated. Here, we developed *Gkn2* knockout and transgenic overexpressing mice to investigate the functional impact of GKN2 loss in GC pathogenesis. In mouse models of GC, decreased GKN2 expression correlated with gastric pathology that paralleled human GC progression. At baseline, *Gkn2* knockout mice exhibited defective gastric epithelial differentiation but not malignant progression. Conversely, *Gkn2* knockout in the IL-11/STAT3-dependent *gp130*$^{F/F}$ GC model caused tumorigenesis of the proximal stomach. Additionally, gastric immunopathology was accelerated in *Helicobacter pylori*–infected *Gkn2* knockout mice and was associated with augmented T helper cell type 1 (Th1) but not Th17 immunity. Heightened Th1 responses in *Gkn2* knockout mice were linked to deregulated mucosal innate immunity and impaired myeloid-derived suppressor cell activation. Finally, transgenic overexpression of human gastrokines (GKNs) attenuated gastric tumor growth in *gp130*$^{F/F}$ mice. Together, these results reveal an antiinflammatory role for GKN2, provide in vivo evidence that links GKN2 loss to GC pathogenesis, and suggest GKN restoration as a strategy to restrain GC progression.

Introduction

Gastric cancer (GC) has one of the highest rates of neoplasia-related mortality worldwide (1). Chronic inflammation after infection with *Helicobacter pylori* is an established risk factor for the most common or "intestinal-type" GC (2), initiating progression to atrophic gastritis, intestinal metaplasia, and adenocarcinoma (2). Nevertheless, causal mechanisms linking inflammation to GC progression remain incompletely understood. GC is believed to be of epithelial origin, deriving clonally from gastric epithelial cells (GECs) or their progenitors (3, 4). Therefore, elucidation of factors that counteract the immune-related premalignant transformation of GECs (2) is of high priority for the advancement of GC therapies and improved survival.

Gastrokines (GKNs) are small (~18-kDa) proteins belonging to the BRICHOS protein superfamily, characterized by an approximately 100–amino acid BRICHOS domain, with established links to inflammatory disease, dementia, and cancer (5, 6). While all BRICHOS proteins are secreted or processed to generate secreted mature peptides, GKNs are unique in being almost exclusively expressed within, and secreted by, mucus-producing epithelial cell lineages of the stomach (6–9). The 3 GKNs are encoded by a tightly linked gene cluster on human chromosome 2p13.3 and show broad evolutionary conservation in mammals and higher vertebrates (6, 10). *GKN1* and *GKN2* were identified in differential expression screens as novel genes downregulated in GC (7, 8, 11). The recently discovered *GKN3* was found in a bioinformatic scan for novel BRICHOS proteins. Mouse *Gkn3*, in contrast to the other GKNs, is overexpressed in atrophic gastritis associated with *H. pylori* infection (9, 10). While broadly functional in mammals, human *GKN3* persists only as a nonexpressed pseudogene (9, 10).

Abundantly expressed in surface mucus cells (SMCs) of the normal human stomach, GKN1 and GKN2 show coordinate downregulation in *H. pylori* infection, frequent loss of expression in gastric adenocarcinoma, and silencing in tumor cell lines (8). Conversely, an expression microarray study identified *GKN2* as the most upregulated gene in the gastric transcriptome after eradication of *H. pylori* and resolution of mucosal inflammation (12). These observations argue that GKNs and, in particular, GKN2, function either as homeostatic regulators of mucosal immunity and/or as stomach-specific tumor-suppressor genes (TSGs). Bioactivities attributed to GKNs include growth suppression, inhibition of epithelial-to-mesenchymal transition, migration, and invasion of tumor cells (reviewed in ref. 6). While ostensibly supportive of TSG or anticancer roles, these functional observations derive

Conflict of interest: The authors have declared that no conflict of interest exists.
Submitted: May 12, 2015; **Accepted:** February 4, 2016.
Reference information: *J Clin Invest*. 2016;126(4):1383–1400. doi:10.1172/JCI82655.

mostly from studies in transformed cell lines and, thus, have limited in vivo relevance. Modes of action of GKNs are poorly understood, with cognate receptors and signal transduction pathways remaining elusive (see commentary in ref. 6). However, reports of a gastric secreted GKN2/trefoil factor 1 (TFF1) heterodimer (13, 14) have suggested that GKN2 might act via homeostatic and/or tumor-suppressor activities of TFFs. Current literature implicates GKN2 loss as a determinant of GC pathogenesis, yet evidence of a causal role is lacking. Despite their likely clinical importance, none of the GKNs have been tested functionally in mouse genetic models. As such, physiological and pathological roles of GKN2 (and of other GKNs) remain unsubstantiated in vivo.

To address the impact of GKN2 loss on GC pathogenesis in vivo, here we report the generation and phenotype analysis of *Gkn2* knockout mice. Our studies show that GKN2 has antiinflammatory activity in the stomach sufficient to restrain progression of cytokine-driven gastric tumorigenesis and *H. pylori* infection–related premalignancy. Moreover, transgenic expression of human GKNs in a validated gastric tumor model restrains pathological progression. The mechanism for GKN2 activity involves expansion and activation of suppressive myeloid cells and inhibition of antigen-presenting cells (APCs), including macrophages and DCs, leading to, leading to attenuated mucosal Th1 immunity. These studies reveal anti-inflammatory and tumor inhibitory roles for GKN2 and elucidate GKN2 loss as a key event underlying GC progression.

Results

Conserved GKN2 expression loss in human and mouse GC progression. Human *GKN2* and mouse *Gkn2* are highly conserved in their genomic organization, intron/exon structure, and genetic linkage to other GKN paralogs (Supplemental Figure 1; supplemental material available online with this article; doi:10.1172/JCI82655DS1) and are thus predicted to show similar regulation in vivo. Mouse genetic models have revealed key mechanisms underlying the premalignant transformation of GECs (15–19) and collectively reproduce many of the histopathologic features of human GC progression (Supplemental Figure 2). To confirm clinical relevance and establish a rationale for using a mouse genetic approach to GKN2 loss, we compared *GKN2* expression in human and mouse GC pathogenesis. Quantitative RT-PCR (QRT-PCR) revealed progressive loss of *GKN2* mRNA in human gastric epithelial tissues from individuals with *H. pylori* infection/gastritis (fold change –3.61 ± 0.56; $P < 0.001$) and intestinal metaplasia (fold change –10.62 ± 3.51; $P < 0.001$) relative to normal (disease-free) controls; *GKN2* mRNA was either marginally expressed or undetected in the majority of gastric tumors (GC; fold change –84,223 ± 31,909; $P < 0.001$; Figure 1A). Loss of *GKN2* mRNA was also reflected at the protein level. Immunohistochemical staining revealed abundant GKN2 expression in SMCs of normal antral mucosa, whereas GKN2 expression was reduced in *H. pylori*–infected tissues and absent in the majority of intestinal metaplasia and GC tissues (Figure 1B).

In mice, GKN2 protein was also stomach specific (Figure 1C), and, as previously shown in humans (15), it localized to SMCs of the gastric corpus and antrum (Figure 1D). We assessed *Gkn2* mRNA expression levels in mouse *H. pylori* infection, transgenic, and knockout models, which collectively reproduce *H. pylori* inflammatory, premalignant, and tumorigenic stages of human GC. QRT-PCR revealed progressive loss of *Gkn2* mRNA from the proximal or corpus stomach, commencing between 7 days and 2 months after infection (MPI) with mouse-adapted *H. pylori* Sydney strain 1 (SS1), with more pronounced loss (in whole stomach) at 12 MPI (Figure 1E). Similarly, decreased *Gkn2* mRNA expression occurred in stomachs of mice with genetic induction of gastric inflammation (stomach-overexpressing H^+K^+ATPase β subunit [*Atp4b*] promoter *Gm-CSF* transgenic [*Gm-CSF*^{Tg}] mice), atrophy/metaplasia/hypertrophy (*HK*$\beta^{-/-}$ mice), and tumorigenesis (*gp130*$^{F/F}$ mice; *HK*β promoter *IL1*β transgenic [*IL1*β^{Tg} mice]) (Figure 1F). *Gkn2* mRNA expression was unchanged in the distal (antral) stomach during the early stages of *H. pylori* infection (7 days and 2 MPI; Figure 1E) but strongly downregulated in antral tumors of *gp130*$^{F/F}$ mice (Figure 1F). Therefore, *GKN2*/*Gkn2* expression levels were inversely correlated with (*H. pylori*–related) gastric pathology. These results reveal conservation of GKN2 loss in GC pathogenesis in humans and mice, thereby validating a mouse genetic approach to investigate GKN2 loss in vivo.

Targeted deletion of the mouse Gkn2 locus. We derived a *Gkn2* knockout allele using VelociGene embryonic stem cell lines (Knockout Mouse Project) in which *Gkn2*-coding exons were replaced with a *lacZ* reporter and floxed neomycin selection cassette. The neomycin cassette was excised by crossing *Gkn2*$^{+/-}$ heterozygotes with germline-specific Cre-recombinase–deleter transgenic mice (20), and the resulting progeny were mated to obtain homozygous mutants (Figure 2, A and B). Homozygous *Gkn2*$^{-/-}$ mice were functionally null, showing a complete absence of GKN2 protein in gastric lysates, but expressed normal levels of GKN1 and GKN3 proteins (Figure 2C). Additionally, *Gkn2*$^{-/-}$ mice showed normal fertility, viability, and postnatal survival (Supplemental Tables 1 and 2 and Supplemental Figure 3). To identify cell lineages primarily affected by targeting the *Gkn2* locus, we histochemically assessed *lacZ* reporter gene (β-gal) expression by staining whole-mount stomachs with X-gal (Supplemental Methods). Consistent with the pattern of endogenous *Gkn2* expression (Figure 1D), we observed intense β-gal expression in the corpus and antral-pyloric mucosa of *Gkn2*$^{+/-}$ mice (Figure 2, D and E), which ceased abruptly at the proximal limiting ridge at the corpus/forestomach (Figure 2F) and pyloric/duodenal (Figure 2G) junctions, respectively. Histological analysis showed specific localization of β-gal expression to SMCs of the corpus (Figure 2, H and I) and antrum (Figure 2, J and K). Double staining in *Gkn2*$^{+/-}$ stomachs confirmed overlapping distribution of GKN2 and β-gal in SMCs (Figure 2, L–N). Therefore, expression of this *Gkn2-lacZ* reporter/null allele mirrors that of endogenous GKN2 protein, suggesting that gastric SMC is the only lineage autonomously affected by GKN2 loss of function in *Gkn2*$^{-/-}$ mice.

Gkn2$^{-/-}$ *mice show impairment of gastric epithelial differentiation that does not progress to malignant disease*. Stomachs from 6-, 12-, and 30-week-old *Gkn2*$^{-/-}$ mice were examined by standard histopathology. Although cell-autonomous TSG roles have been long suspected of GKN family proteins (6), *Gkn2*$^{-/-}$ mice showed no evidence of spontaneous gastric tumors to support this supposition. *Gkn2*$^{-/-}$ mice presented with clear abnormalities of the corpus mucosa, including focal hypertrophic lesions, which were evident macroscopically and histologically. Lesions were first apparent at 6 weeks of age and persisted, but did not increase in severity, in

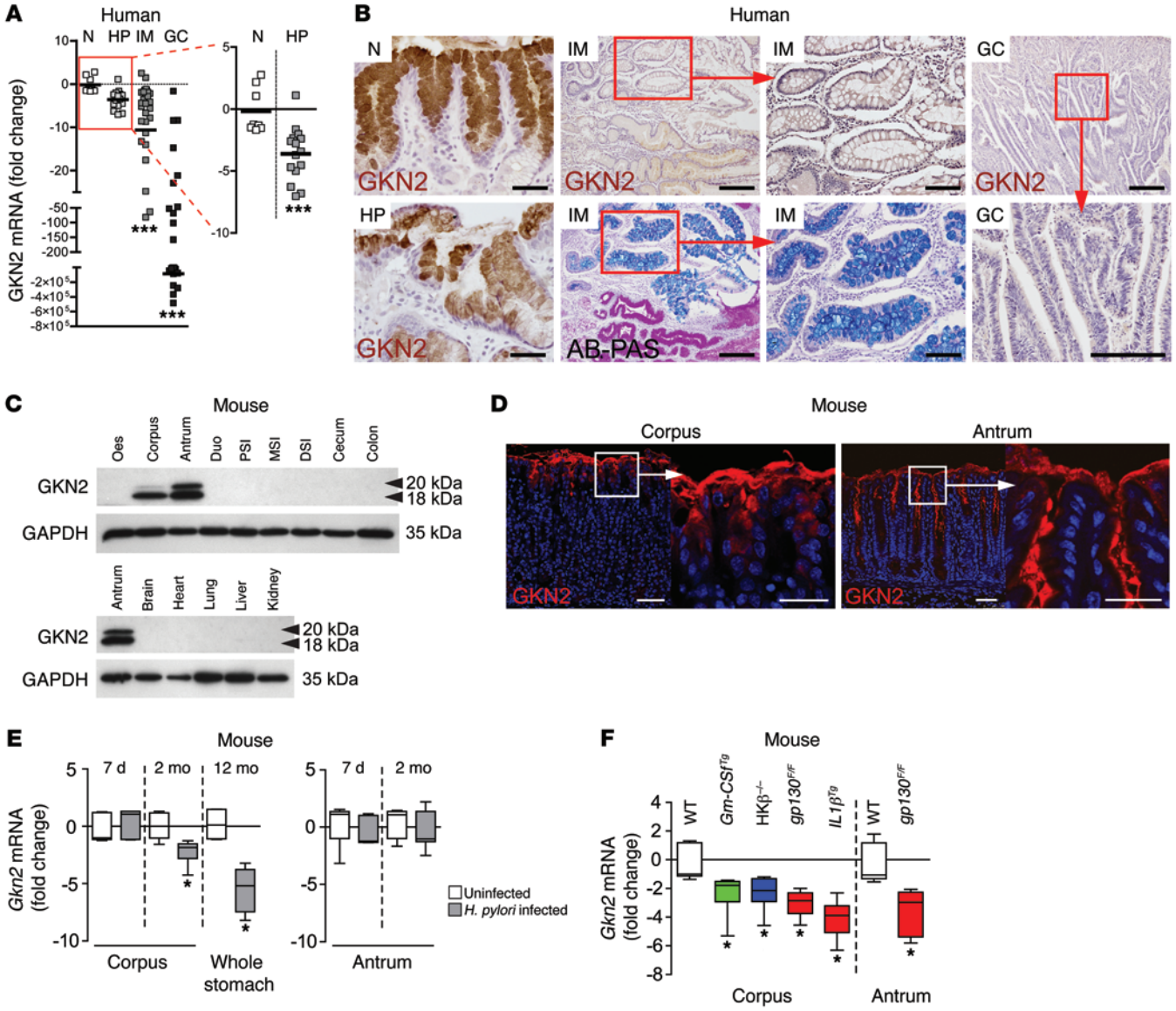

Figure 1. Loss of *GKN2* expression in human and mouse GC progression. (**A**) QRT-PCR analysis of *GKN2* mRNA in human GC. Scatter plots show mRNA fold changes for *H. pylori*–infected tissue (HP; $n = 16$), premalignant tissue adjacent to tumor with intestinal metaplasia (IM; $n = 28$), and GC tissue ($n = 28$) relative to normal (N; $n = 6$) gastric epithelial tissues. (**B**) Representative photomicrographs showing GKN2 immunostaining in human gastric tissues (see above). Normal and *H. pylori*–infected tissue show antral mucosa. Scale bar: 50 μm. Intestinal metaplasia shows corpus mucosa; presence of goblet cells is confirmed by AB-PAS staining of an adjacent section. GC shows adenocarcinoma in corpus mucosa. Scale bar: 100 μm (first and second columns and top image fourth column); 50 μm (third column and bottom image fourth column). (**C**) Immunoblots of mouse GKN2 protein. GAPDH verifies protein integrity. Two GKN2 bands represent unprocessed precursor (20-kDa) and secreted mature (18-kDa) protein, respectively. Oes, oesophagus; Duo, duodenum; PSI, proximal small intestine; MSI, middle small intestine; DSI, distal small intestine. (**D**) Immunofluorescent localization of mouse GKN2 protein in corpus and antrum mucosa. Scale bar: 50 μm (first and third image) and 25 μm (second and fourth image). (**E**) QRT-PCR analysis of *Gkn2* mRNA in *H. pylori* SS1–infected WT (C57BL/6) mouse corpus, antrum, or whole stomach at 7 days (7 d), 2 months (2 mo), or 12 months (12 mo). Box plots show median mRNA fold change relative to uninfected mice. (**F**) QRT-PCR analysis of mouse genetic models described in **B**. (**E** and **F**) In box-and-whisker plots, horizontal bars indicate the medians, boxes indicate 25th to 75th percentiles, and whiskers indicate 10th and 90th percentiles. *P* values were determined using a 2-tailed Student's *t* test: $^*P < 0.05$; $^{***}P < 0.001$.

12- and 30-week-old animals (Figure 3, A and B, and Supplemental Figure 4). Mucosal defects, including inflammation, glandular atrophy, mucus neck cell (MNC) hyperplasia, and replacement of periodic acid–Schiff–stained (PAS-stained) neutral mucin with Alcian blue–stained acidic mucin in SMC (SMC metaplasia), were all significantly increased in the corpus mucosa of 6- and 12-week-old *Gkn2*$^{-/-}$ mice, while MNC hyperplasia and SMC metaplasia remained significantly elevated in 30-week-old *Gkn2*$^{-/-}$ mice (Figure 3C). Overall corpus mucosal thickness in *Gkn2*$^{-/-}$ mice was not significantly different than that of age-matched WT mice (Figure 3D). Nonetheless, corpus mucosal defects, and lesion areas in particular, were associated with an increased epithelial proliferation rate in 6- and 12-week-old but not 30-week-old *Gkn2*$^{-/-}$ mice (Figure 3E). By contrast, the antral mucosa of *Gkn2*$^{-/-}$ mice had a

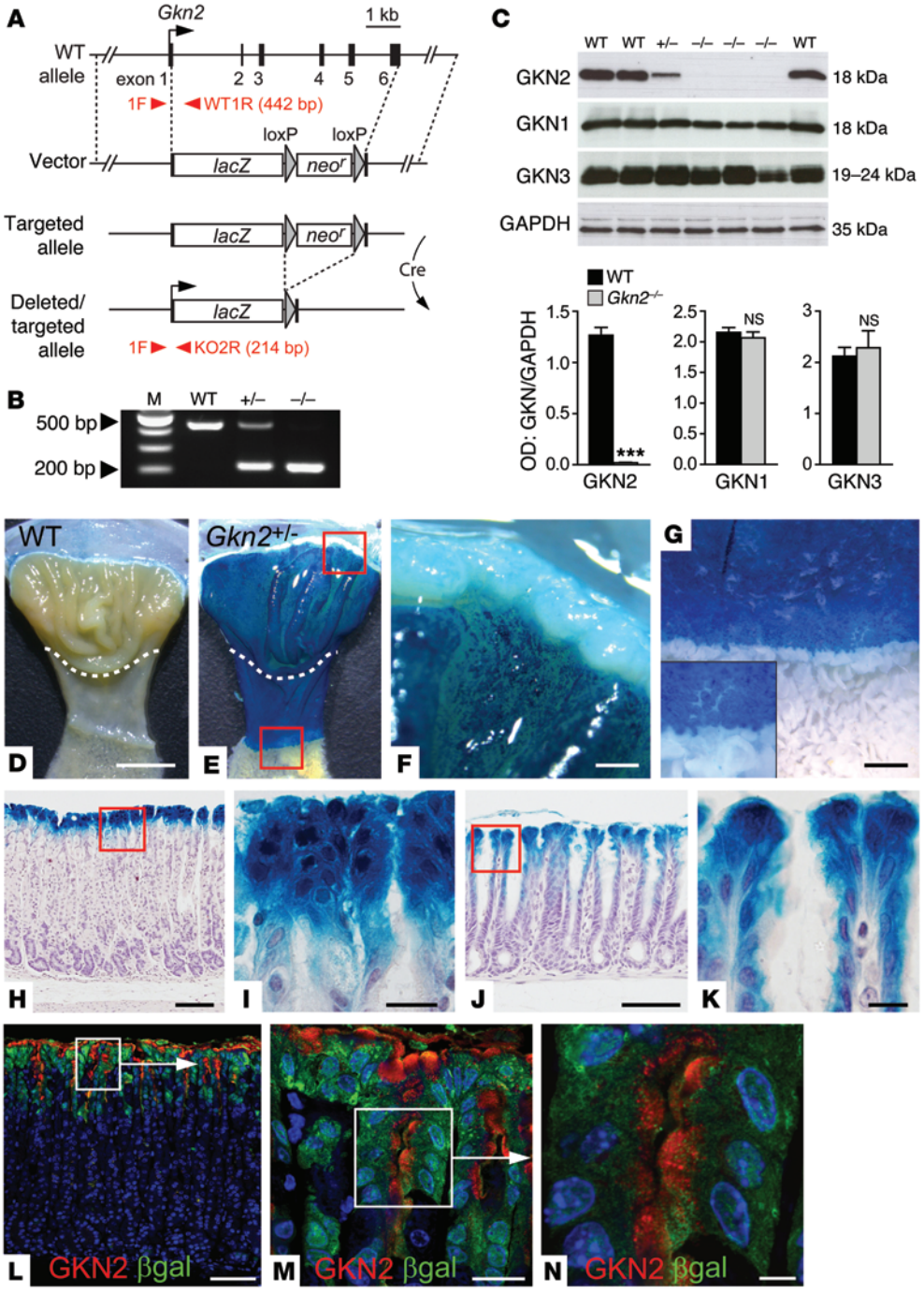

Figure 2. Targeted deletion of the mouse *Gkn2* locus. (**A**) Strategy used to target the mouse *Gkn2* locus. Red arrowheads denote primer pairs used to amplify WT and targeted alleles by PCR. Scale bar: 1 kbp. (**B**) PCR genotyping strategy. WT and targeted alleles generate 442-bp and 214-bp bands, respectively. Upper and lower bands show 500 and 200 bp, respectively. M, molecular weight marker of the 100-bp ladder. (**C**) Immunoblot showing GKN2 protein expression in WT, *Gkn2*$^{+/-}$, and *Gkn2*$^{-/-}$ gastric corpus tissues. Molecular weights (kDa) of protein bands are shown. Histograms show densitometry of protein bands/GAPDH (n = 3 per group). P values were determined using a 2-tailed Student's t test: ***$P < 0.001$. (**D**–**K**) β-Gal reporter activity in *Gkn2*$^{+/-}$ and WT stomachs stained with X-gal (bright blue stain). (**D** and **E**) Macroscopic images of X-gal–stained stomachs. Boxed areas are shown at higher magnification in **F** and **G**. Scale bar: 5 mm. (**F** and **G**) High-magnification images showing (**F**) proximal and (**G**) distal extents of β-gal staining in *Gkn2*$^{+/-}$ stomachs. Scale bar: 500 μm. Original magnification, ×2 (inset). (**H**–**K**) Histological images of (**H** and **I**) corpus and (**J** and **K**) antral β-gal staining in *Gkn2*$^{+/-}$ stomachs (dark blue), with hematoxylin counterstain (pale blue). Scale bar: 50 μm (**H** and **J**); 20 μm (**I** and **K**). (**L**–**N**) Immunofluorescent colocalization of GKN2 and β-gal proteins in *Gkn2*$^{+/-}$ corpus mucosa. Boxed areas are shown at higher magnification in **M** and **N**. Scale bar: 50 μm (**L**); 20 μm (**M**); 5 μm (**N**).

normal histological structure, thickness, and epithelial proliferation count (Figure 3, A, B, D, and E). A detailed study of gastric epithelial markers and cellular changes underlying atrophy and metaplasia was performed in 12-week-old *Gkn2*$^{-/-}$ mice (in which mucosal lesions and glandular defects are most pronounced). Expression of the gastric trefoil factor (*Tff1*, *Tff2*) and mucin genes (*Muc1*, *Muc5ac*, *Muc6*) was not significantly altered, at least in bulk gastric tissue (Figure 4A). However, the SMC metaplasia (showing ectopic Alcian blue staining) was associated with a selective loss of MUC5AC, but not TFF1, specifically within lesion areas by immunofluorescent staining (Figure 4B). Similarly, MNC hyperplasia and glandular atrophy were, respectively, characterized by quantifying expansion of MNC zone and cellular loss within both parietal cell and zymogenic cell compartments (Figure 4C). The modest reduction in parietal cell number was not associated with changes in either stomach acid content (Figure 4D and Supplemental Methods) or antral expression of gastrin (Figure 4E), the principal endocrine stimulator of acid production. Collectively, we believe that these results identify GKN2 as a novel regulator of gastric epithelial homeostasis.

Proximal gastric tumorigenesis in GKN2-deficient gp130$^{F/F}$ *mice*. Given the role of GKN2 in maintenance of gastric epithelial homeostasis, we asked whether GKN2 genetic loss might potentiate the effects of oncogenic pathways known to induce gastric epi-

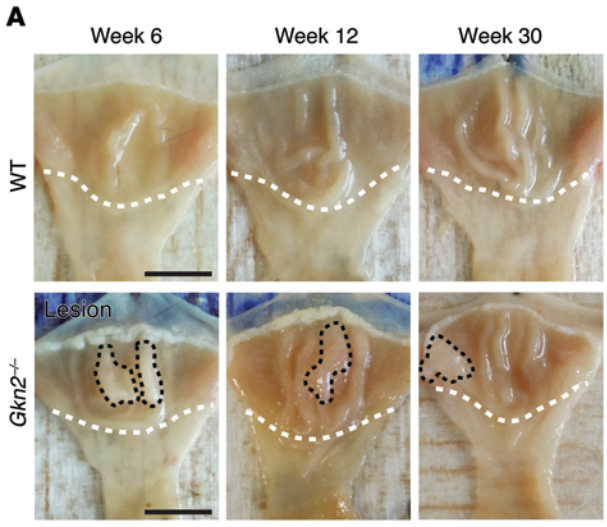

Figure 3. *Gkn2*$^{-/-}$ mice display impaired basal gastric epithelial differentiation. (**A**) Representative images of the gastric mucosa of 6-, 12-, and 30-week-old *Gkn2*$^{-/-}$ and WT littermate control mice. Boundaries between corpus and antral mucosae are delineated with white dashed lines; hypertrophic mucosal lesions are shown by black dashed lines. Scale bar: 5 mm. (**B**) Low-power images showing AB-PAS–stained *Gkn2*$^{-/-}$ hypertrophic lesions compared with nonlesion and WT corpus mucosa. Scale bar: 200 μm. High-power images of corpus and antrum mucosa in 12-week-old *Gkn2*$^{-/-}$ and WT mice. Scale bar: 50 μm. (**C**) Summary of semiquantitative histopathology scores for corpus inflammation (inflamm), atrophy, MNC hyperplasia (MNC hyp), and SMC metaplasia (SMC met) in 6-, 12-, and 30-week-old WT and *Gkn2*$^{-/-}$ mice (group sizes as stated in **D**). (**D**) Morphometric analysis of corpus and antral mucosal thickness in 6-, 12-, and 30-week-old *Gkn2*$^{-/-}$ (n = 11, n = 9, n = 7) and WT mice (n = 7, n = 9, n = 8). Histograms show mean mucosal thickness as histological cross-sectional area/mm^2 per mm length of muscularis mucosae. (**E**) Ki-67 labeling of proliferating cells in corpus mucosa of 6-, 12-, and 30-week-old WT and *Gkn2*$^{-/-}$ mice and antral mucosa of 12-week-old WT and *Gkn2*$^{-/-}$ mice (n = 6 per group). Representative images of 12-week-old WT and *Gkn2*$^{-/-}$ corpus and *Gkn2*$^{-/-}$ lesion mucosa are shown. Scale bar: 100 μm. Error bars represent mean ± SEM. P values were determined using a 2-tailed Student's t test: $^*P < 0.05$; $^{**}P < 0.01$; $^{***}P < 0.001$.

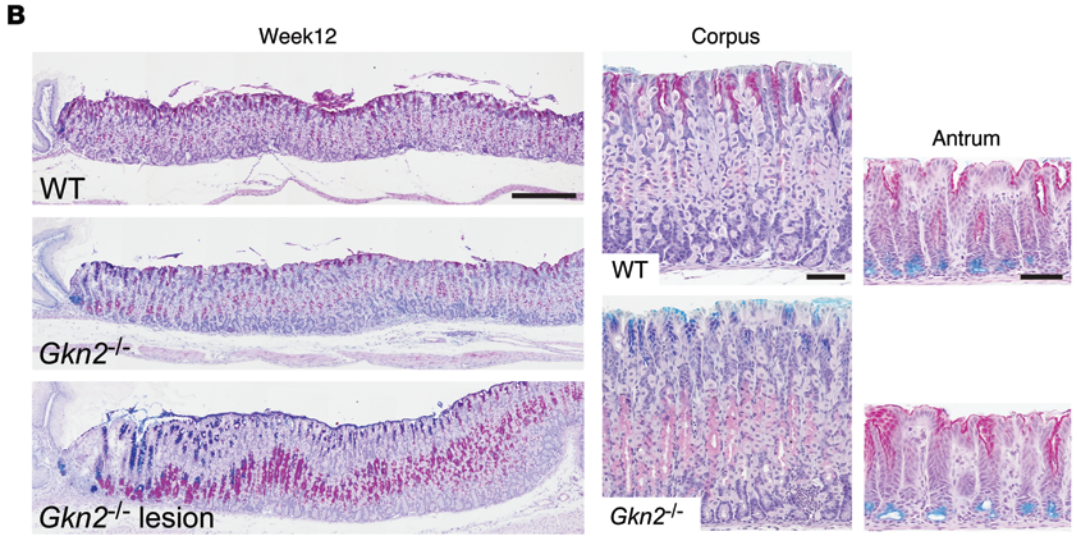

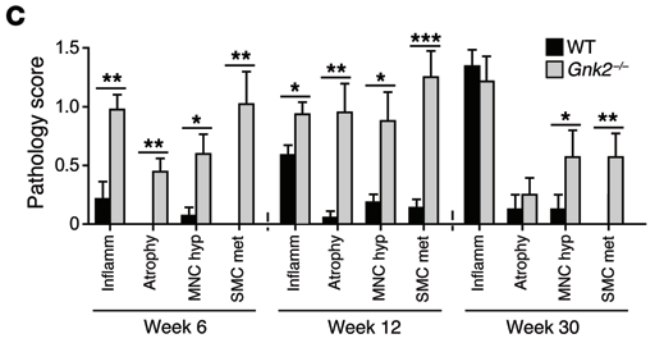

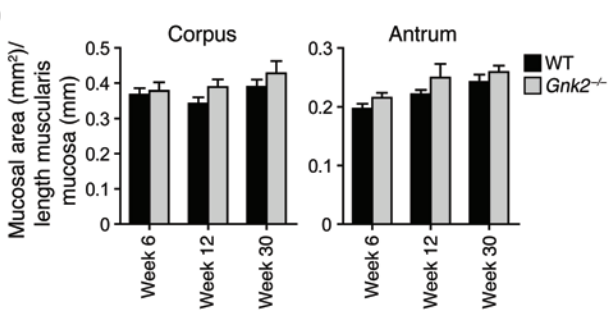

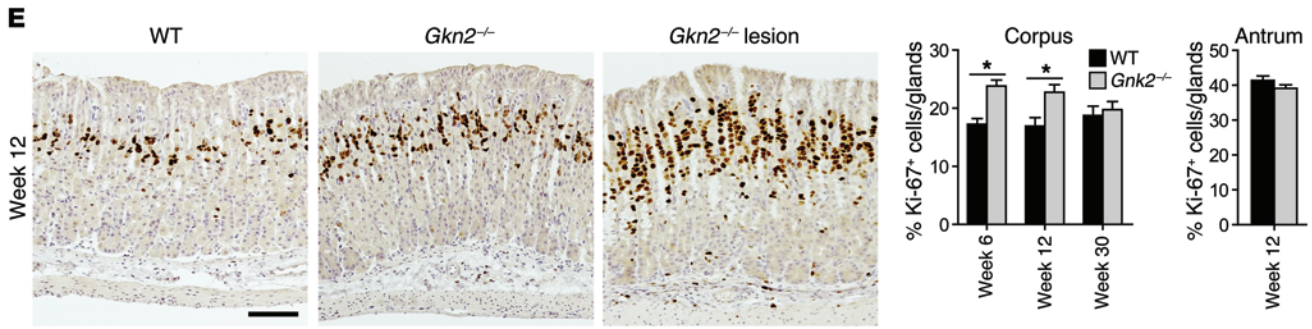

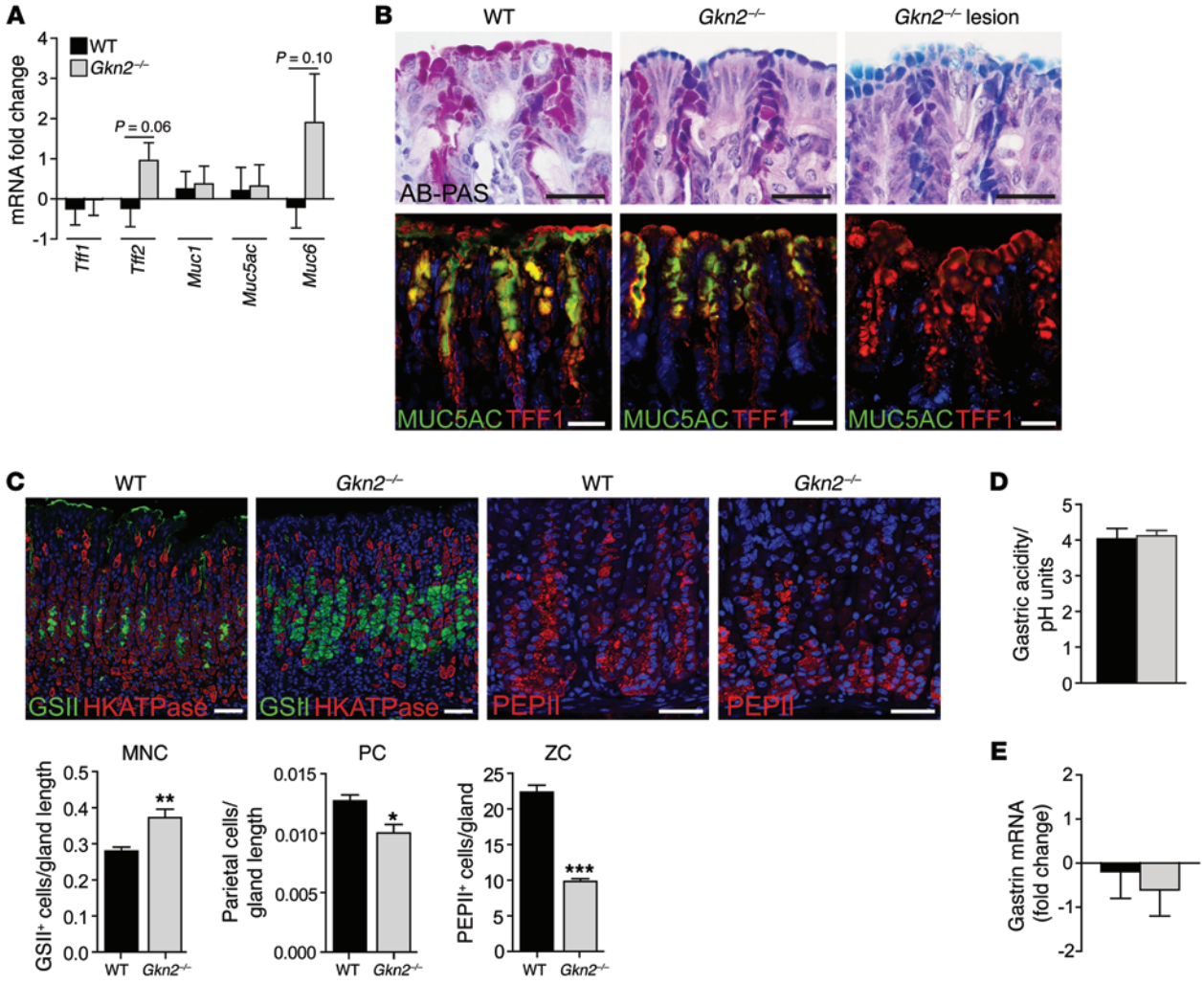

Figure 4. Cellular and molecular analysis of gastric epithelial differentiation in *Gkn2*$^{-/-}$ mice. (**A**) Expression of gastric trefoil factor and mucin genes in 12-week-old *Gkn2*$^{-/-}$ (n = 11) and WT (n = 8) corpus by QRT-PCR. (**B**) Characterization of SMC differentiation in 12-week-old WT and *Gkn2*$^{-/-}$ corpus and *Gkn2*$^{-/-}$ lesion mucosa by AB-PAS staining (top row) and immunofluorescent staining for MUC5AC and TFF1 proteins (bottom row). Scale bar: 20 μm. (**C**) Immunofluorescent quantitation of MNCs (MNC, GSII); parietal cells (PC, HK ATPase-β); and zymogenic cells (ZC, pepsinogen II) in 12-week-old WT and *Gkn2*$^{-/-}$ corpus mucosa (n = 6 per group). Scale bar: 20 μm. (**D**) Gastric acidity determined by pH measurement of stomach contents in *Gkn2*$^{-/-}$ (n = 11) and WT (n = 8) mice. (**E**) QRT-PCR analysis of gastrin mRNA expression in antral stomachs of *Gkn2*$^{-/-}$ (n = 11) and WT (n = 8) mice. Error bars represent mean ± SEM. P values were determined using a 2-tailed Student's t test: $^{*}P < 0.05$; $^{**}P < 0.01$; $^{***}P < 0.001$.

thelial tumors in mice. The IL-11/gp130/STAT3 axis is a key driver of GC pathogenesis (15, 16). Mice carrying a knockin mutation at the gp130 cytokine coreceptor locus (*gp130*$^{F/F}$) show STAT3 hyperactivation and spontaneous tumorigenesis in the antrum, which progresses to encompass the entire secretory mucosa. In the antral stomach, gp130/STAT3 activation is dependent on the cytokine IL-11 (21–23), and the knockin mutant progresses through chronic inflammation, metaplasia, and dysplasia to carcinoma in situ, phenocopying all but the metastatic stage of human intestinal-type GC development (16). In contrast to *gp130*$^{F/F}$ single mutants, which mainly show antral tumors, *Gkn2*$^{-/-}$ *gp130*$^{F/F}$ compound mutants additionally showed extensive focal tumorigenesis of the corpus and squamous epithelium overlying the limiting ridge of the corpus/forestomach junction at 12 weeks of age (Figure 5A). This phenotype was supported quantitatively by an increase in the number of corpus tumor foci (Figure 5B) and an increased macroscopic corpus tumor area in *Gkn2*$^{-/-}$ *gp130*$^{F/F}$ mice (Figure 5C). Histological analysis of the tumors revealed a poorly differentiated and hyperplastic epithelium (Figure 5, D and E), contributing to a significant increase in corpus mucosal thickness overall (Figure 5F). In contrast, the antral tumor load and mucosal thickness in *Gkn2*$^{-/-}$ *gp130*$^{F/F}$ mice were not significantly different than those of *gp130*$^{F/F}$ single mutants (Figure 5, A, C, and F). To further characterize the corpus tumor lineage, we examined the β-gal reporter expression profile of *Gkn2*$^{-/-}$ *gp130*$^{F/F}$ stomach tissues by staining with X-gal. Strikingly, while adjacent normal mucosa retained strong reporter expression, corpus (and antral) tumors were comprised predominantly by unstained cells (Figure 6, A–E). Consistent with the absence of reporter expression (which marks the SMC lineage), the tumors also lacked MUC5AC staining, although TFF1 expression was retained, while both proteins were abundantly expressed in adjacent nontumoral mucosa (Figure 6, F and

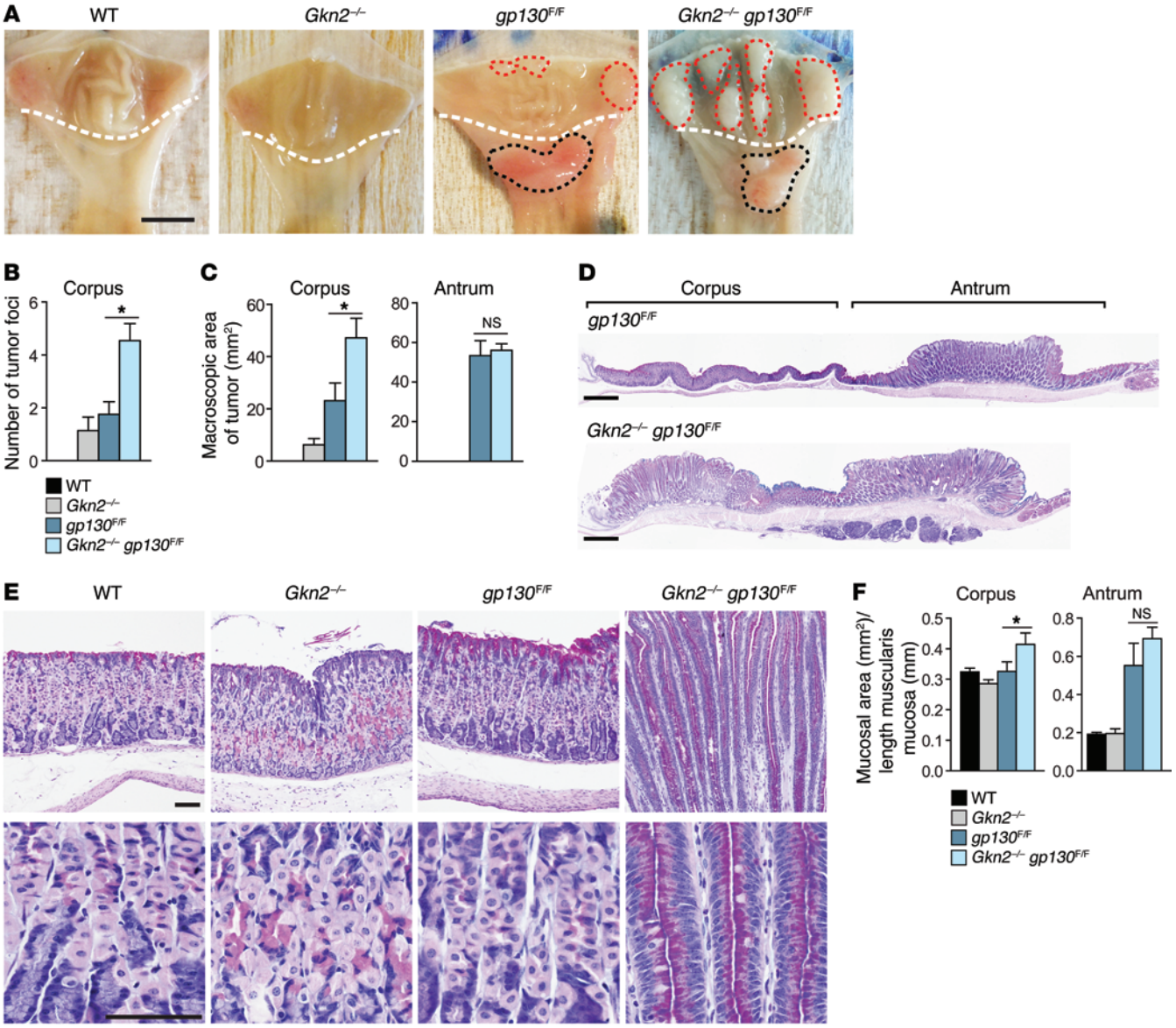

Figure 5. Proximal stomach tumorigenesis in *Gkn2*$^{-/-}$ *gp130*$^{F/F}$ compound mutant mice. (**A**) Representative images of corpus and antral tumor phenotypes in 12-week-old *Gkn2*$^{-/-}$ *gp130*$^{F/F}$ compound mutants (n = 13) compared with *gp130*$^{F/F}$ (n = 5) and *Gkn2*$^{-/-}$ single mutants (n = 12) and WT (n = 6) littermate control mice. White dashed lines delineate boundaries between corpus and antrum; tumor areas are shown by red (corpus) or black (antral) dashed lines. Scale bar: 5 mm. (**B** and **C**) Morphometric analysis of tumor burden in *Gkn2*$^{-/-}$ *gp130*$^{F/F}$ compound mutants. (**B**) Corpus tumor incidence expressed as the number of tumor foci within gastric corpus. (**C**) Macroscopic area of corpus and antral tumors in mm^2. (**D**) Low-power images showing differential tumor histology (AB-PAS staining) in *Gkn2*$^{-/-}$ *gp130*$^{F/F}$ compound mutant and *gp130*$^{F/F}$ single mutant stomachs. Scale bar: 500 μm. (**E**) High-power histological images (original magnification, ×100 [top row]; ×400 [bottom row]) of corpus mucosal defects in *Gkn2*$^{-/-}$ *gp130*$^{F/F}$ mice stained with AB-PAS. Scale bar: 50 μm. (**F**) Morphometric analysis of corpus and antral mucosal thickness in *Gkn2*$^{-/-}$ *gp130*$^{F/F}$ compound mutants. Error bars represent mean ± SEM. P values were determined using a 2-tailed Student's t test: *$P < 0.05$.

H). We found no evidence of mucus metaplasia within the tumor masses, as shown by a lack of TFF2/*Griffonia simplicifolia* lectin II (TFF2/GSII) staining, although clusters of TFF2/GSII-positive cells were seen at the tumor margins and in adjacent nontumoral mucosa (Figure 6, G and I). Similarly, none of the *Gkn2*$^{-/-}$ *gp130*$^{F/F}$ tumors showed evidence of true intestinal metaplasia, as evidenced by absence of CDX2 expression (Figure 6, I and J).

Absence of synergistic phenotypes in compound mutant Gkn2$^{-/-}$ *Tff1*$^{-/-}$ *mice.* We examined the effect of GKN2 genetic deficiency in the *Tff1*$^{-/-}$ gastric tumor model. Our rationale was 3-fold: (a) *Tff1*$^{-/-}$ mice show gastric epithelial hyperplasia progressing to antral tumorigenesis at 3 to 6 months of age (17); (b) TFF1 shows closely overlapping cellular expression with GKN2 (13), raising the possibility of potentiation of individual pathological outcomes; (c) GKN2 and TFF1 have been reported to form heterodimers (14), suggesting cooperative function. Compound mutant *Gkn2*$^{-/-}$ *Tff1*$^{-/-}$ mice showed no differences in tumor incidence, mucosal thickness, or temporal progression at 12 weeks of age compared with single mutant *Tff1*$^{-/-}$ or *Gkn2*$^{-/-}$ mice (Supplemental Figure 5). Therefore, GKN2 deficiency does not significantly influence tumorigenesis in *Tff1*$^{-/-}$ mice and vice versa,

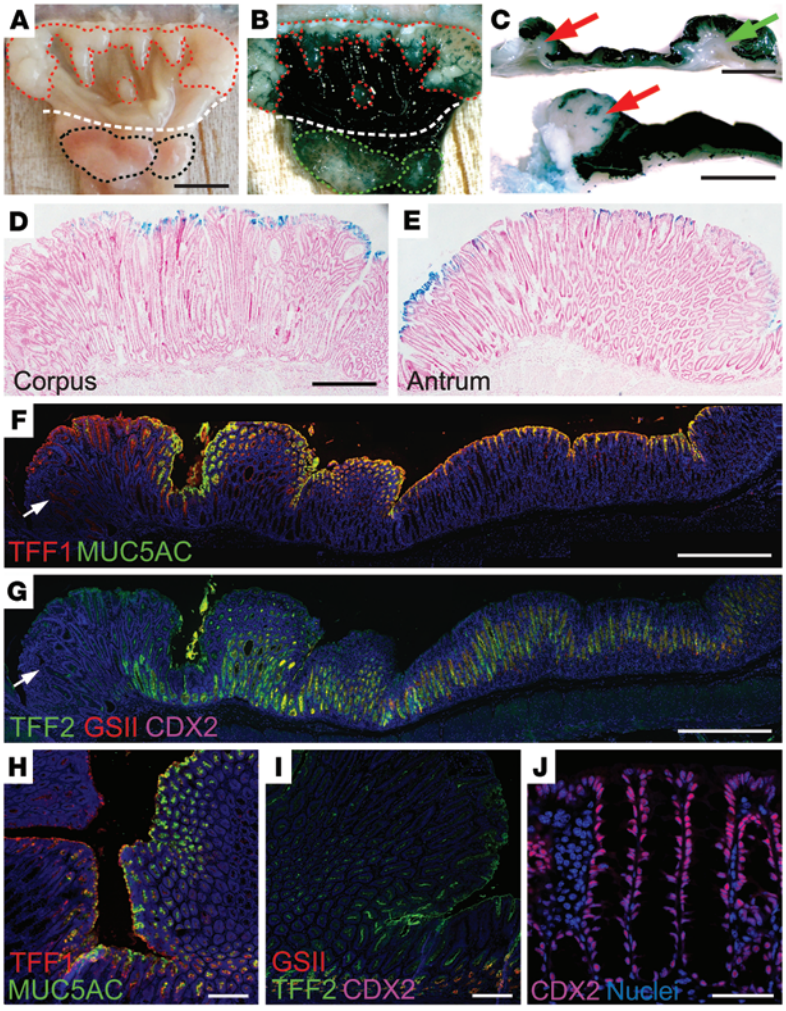

Figure 6. Analysis of gastric and intestinal differentiation in *Gkn2*$^{-/-}$ *gp130*$^{F/F}$ proximal stomach tumors. (**A**–**C**) β-Gal reporter gene expression in *Gkn2*$^{-/-}$ *gp130*$^{F/F}$ gastric corpus tumors. Representative *Gkn2*$^{-/-}$ *gp130*$^{F/F}$ stomach shown (**A**) before and (**B**) after X-gal staining. Tumor areas are shown by red (corpus) or (**A**) black or (**B**) green (antral) dashed lines. Scale bar: 5 mm. (**C**) Lateral images of X-gal–stained and sagittally bisected *Gkn2*$^{-/-}$ *gp130*$^{F/F}$ stomach tissues. Red (corpus) and green (antral) arrows indicate tumor masses. Scale bar: 3 mm. (**D** and **E**) Histological images of X-gal–stained *Gkn2*$^{-/-}$ *gp130*$^{F/F}$ tumors in (**D**) corpus and (**E**) antrum. Scale bar: 100 μm. (**F** and **G**) Low-power image of (**F**) MUC5AC and TFF1 double immunofluorescent staining and (**G**) TFF2, GSII, and CDX2 triple staining in corpus tumors and adjacent nontumoral mucosa of *Gkn2*$^{-/-}$ *gp130*$^{F/F}$ mice. Scale bar: 200 μm. (**H** and **I**) High-power images showing staining patterns at tumor margin for (**H**) MUC5AC and TFF1 and (**I**) TFF2, GSII, and CDX2. Scale bar: 100 μm. (**J**) CDX2 staining in colonic epithelium (positive control). Scale bar: 50 μm.

arguing that GKN2-TFF1 heterodimers are not, at least in mice, required for individual component suppressive function.

H. pylori–infected Gkn2$^{-/-}$ *mice show accelerated progression to atrophic gastritis and metaplasia*. Having shown that GKN2 restrains the progression of cytokine-driven proximal gastric tumorigenesis, we investigated *Gkn2* genetic loss in the context of *H. pylori*–dependent gastritis, a key premalignant lesion of GC (24). Three independent cohorts of 6- to 8-week-old *Gkn2*$^{-/-}$ and WT control mice were orally infected with *H. pylori* SS1 (25), sacrificed at 2 MPI (Figure 7A), and examined for gastric histopathology. Infected *Gkn2*$^{-/-}$ mice showed increased severity of atrophic gastritis and pervasive frequent Alcian blue–positive mucus metaplasia (consistent with spasmolytic polypeptide expressing metaplasia; ref. 26). By contrast, infected WT mice showed relatively mild inflammatory pathology, infrequent atrophy, and metaplasia (Figure 7B), consistent with the known temporal progression of this infection in C57BL/6 mice (25). Accordingly, infected *Gkn2*$^{-/-}$ mice had higher scores of corpus polymorphonuclear and mononuclear infiltrate, glandular atrophy, and mucus metaplasia, while antral inflammatory scores, though increased from uninfected levels, were similar in *Gkn2*$^{-/-}$ and WT mice (Figure 7C). Consistent with the severity of atrophy and metaplasia, infected *Gkn2*$^{-/-}$ mice showed increased corpus expression of mucin 6 (*Muc6*) mRNA and decreased expression of zymogenic cell and parietal cell lineage markers *Mist1* and *HKβ*, respectively (Figure 7D). Infected *Gkn2*$^{-/-}$ mice also had lower *H. pylori* colonization levels (Figure 7E), which were inversely correlated with gastritis severity (Figure 7F), suggesting preferential immune-mediated reduction in bacterial load and/or loss of niche due to mucosal damage. Collectively, these results demonstrate a previously undescribed antiinflammatory function of GKN2, which suppresses *H. pylori*–related inflammation and premalignant disease progression in the stomach.

Hyperactivated Th1 immunity in H. pylori–infected Gkn2$^{-/-}$ *mice*. *H. pylori*–related gastritis is typically driven by a dual T helper cell type 1 (Th1) and Th17 immune response, while Th1 and Th17 pathways are modulated by Th2 and Treg cytokine responses. To better understand mechanisms underlying augmented inflammatory responses in *Gkn2*$^{-/-}$ mice, we first measured levels of anti–*H. pylori* IgG antibody subclasses. Relative to that in WT mice, infected *Gkn2*$^{-/-}$ mice presented with an antibody response that was skewed toward the IgG2c subclass, which is consistent with an increased Th1 immune response (Figure 8A). To consolidate this finding, we quantified by QRT-PCR expression levels of cytokines and transcription factors that are markers for Th1, Th2, Th17, and Tregs as well as markers of associated M1- and M2-type macrophage responses. Infected *Gkn2*$^{-/-}$ mice expressed higher mRNA levels of proinflammatory Th1 markers *Ifng* and *Tbet* (Figure 8B) as well as the M1-associated *Il1b*, *Il6*, *Il11*, and *Cxcl2* (Figure 8C) and antimicrobial peptide genes *Dmbt1* and *Reg3g* (Figure 8D) compared with infected WT or uninfected controls. *Il10* and *Foxp3* were also preferentially induced, consistent with an attempt by Foxp3^{+} Tregs to limit inflammatory damage ensuing from the elevated Th1 response (Figure 8E). By contrast, neither Th2 (Figure 8F) nor Th17 lineage markers (Figure 8G) showed broad expression differences in infected *Gkn2*$^{-/-}$ mice compared with infected WT mice. Therefore, neither Th2 nor Th17 immunity was differentially activated in infected *Gkn2*$^{-/-}$ mice. However, M2-related arginase 1 (*Arg1*), a key suppressor of T cell responses (27), showed significantly decreased expression in infected *Gkn2*$^{-/-}$ mice (Figure 8F), again

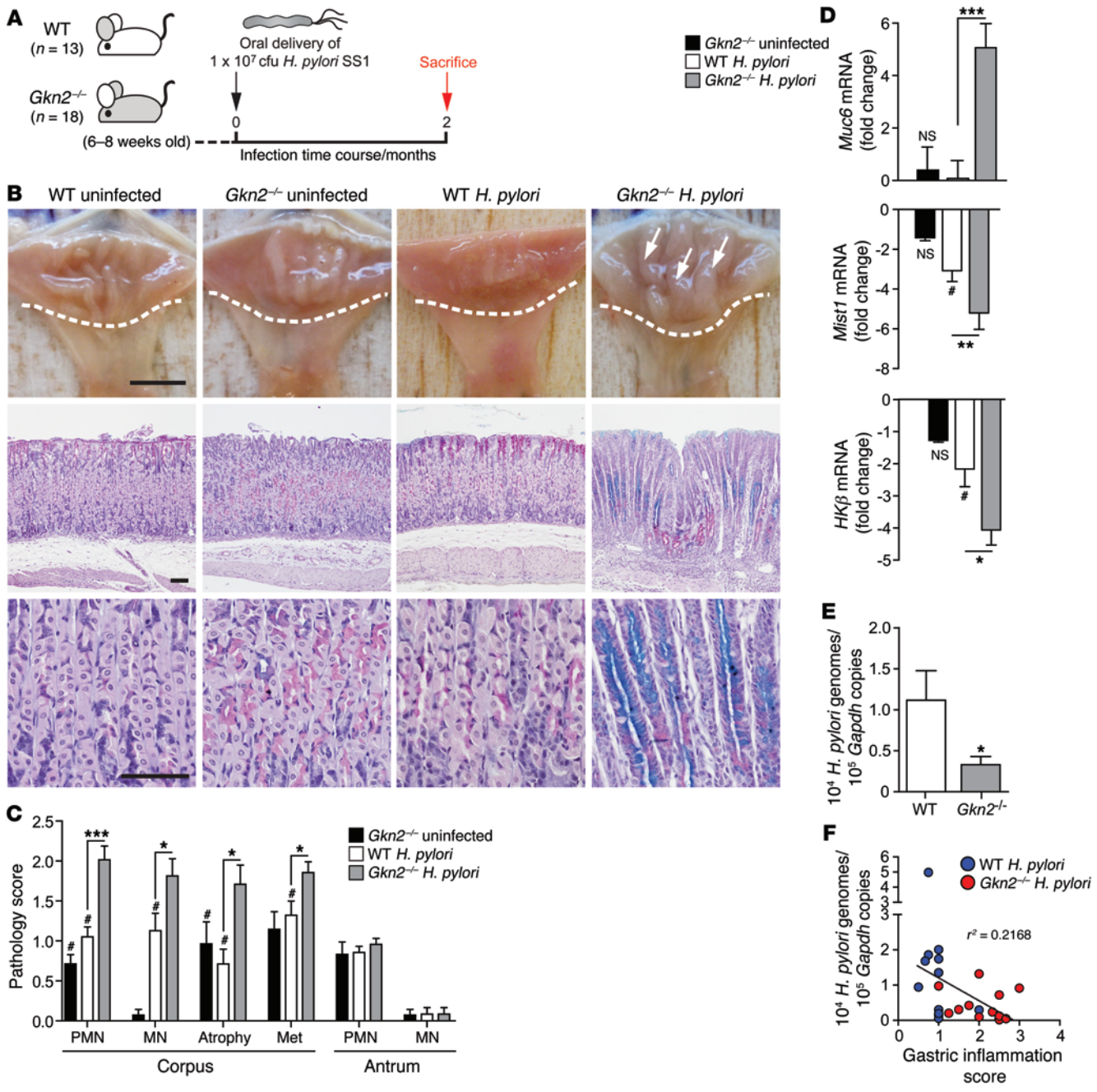

Figure 7. Accelerated progression to atrophic gastritis and mucus metaplasia in *Gkn2*$^{-/-}$ mice after 2-month *H. pylori* infection. (**A**) Strategy used for 2-month *H. pylori* SS1 infections. (**B**) Macroscopic and histological images of *Gkn2*$^{-/-}$ and WT littermate stomachs infected for 2 months and uninfected control stomachs. White dashed lines delineate corpus/antrum boundaries. Arrows show the region of corpus hypertrophy in the infected *Gkn2*$^{-/-}$ stomach macroscopic photo. Scale bar: 5 mm (macroscopic images); 50 μm (histological images). (**C**) Semiquantitative histological assessment of gastric histopathology: inflammatory infiltrate (polymorphonuclear cells [PMN]; mononuclear cells [MN]), atrophy (degree of parietal/zymogenic cell loss), and mucus metaplasia (Met). Histograms show mean pathology scores for each parameter (range 0–4). (**D**) QRT-PCR analysis of metaplasia (*Muc6*) and glandular atrophy–related (*Mist1* and *HKβ*) genes in *Gkn2*$^{-/-}$ mice after 2 months of *H. pylori* infection. Histograms show mean mRNA fold change relative to WT uninfected mice. (**E**) *H. pylori* SS1 colonization levels in stomachs after 2 months of infection, as assessed by Q-PCR (Supplemental Methods). Histograms show mean colonization level (10^4 *H. pylori* genomes per 10^5 *Gapdh* copies). (**F**) Linear regression analysis of corpus inflammation score and colonization level. The correlation coefficient (r^2) value is shown. Error bars represent mean ± SEM. *P* values were determined using a 2-tailed Student's *t* test (**C**) or 2-tailed Mann Whitney U test (**D** and **E**). Statistical significance compared with WT uninfected control mice: $^{\#}P < 0.05$. Statistical significance between treatment groups: $^{*}P < 0.05$; $^{**}P < 0.01$; $^{***}P < 0.001$.

consistent with the proinflammatory phenotype of this model. Given that effects of GKN2 deficiency are predominantly on corpus pathology, none of the above immune markers were differentially expressed in the antra of infected *Gkn2*$^{-/-}$ mice (Supplemental Figure 6). These results indicate that GKN2 restrains gastric immunopathology by modulating Th1, but not Th17, immunity.

Inflammatory phenotype of Gkn2$^{-/-}$ *mice is unrelated to chemokine production by GECs.* Chemokine secretion by epithelial cells

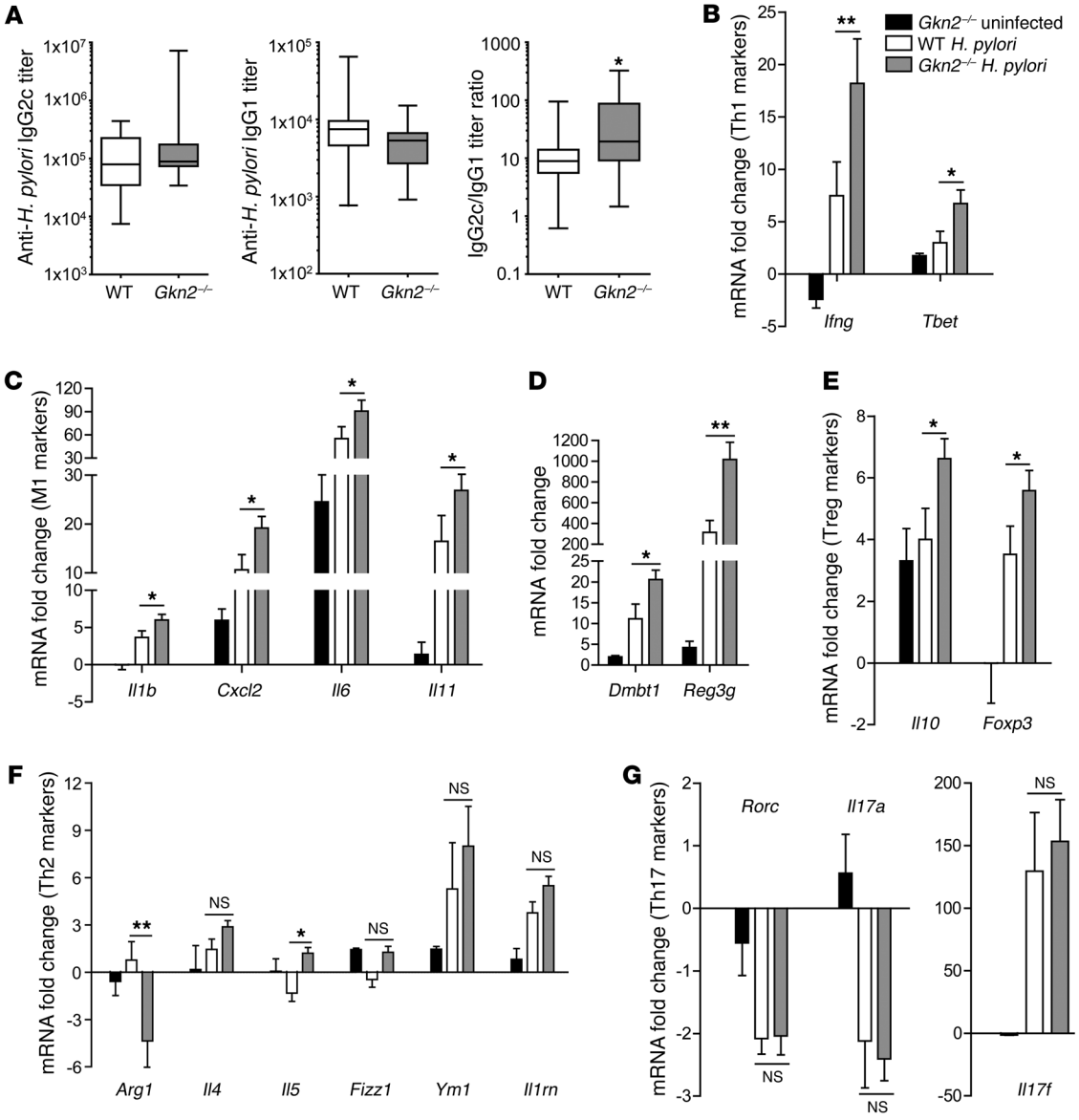

Figure 8. Differential expression of cytokines and immune transcription factors in *Gkn2*$^{-/-}$ mice after 2-month *H. pylori* infection. (**A**) ELISA detection of serum IgG antibody responses in *Gkn2*$^{-/-}$ mice infected for 2 months. Box plots show median (horizontal bars), interquartile range (boxes) and 10th/90th percentile (error bars) titers of individual anti–*H. pylori* IgG2c (Th1) and IgG1 (Th2) and combined IgG2c/IgG1 ratio. (**B**–**F**) QRT-PCR cytokine/chemokine/transcription factor expression profiles of *Gkn2*$^{-/-}$ mice infected for 2 months. (**B**) Th1 markers (*Ifng*, *Tbet*); (**C**) M1 markers (*Il1b*, *Cxcl2*, *Il6*, *Il11*); (**D**) antimicrobial lectins (*Reg3g*, *Dmbt1*); (**E**) Treg markers (*Il10*, *Foxp3*); (**F**) Th2/M2 markers (*Arg1*, *Il4*, *Il5*, *Fizz1*, *Ym1*, *Il1rn*); and (**G**) Th17 markers (*Rorc*, *Il17a*, *Il17f*). Histograms show mean mRNA fold change relative to WT uninfected mice. Error bars represent mean ± SEM. *P* values were determined using a 2-tailed Student's *t* test: $^{*}P < 0.05$; $^{**}P < 0.01$.

is a key mechanism driving myeloid cell recruitment to the gastric mucosa and plays a pivotal role in triggering the host innate response to *H. pylori* infection (28). We hypothesized that GKN2 genetic loss might enhance chemokine release from GECs. To address this, we compared the chemokine/cytokine secretory responses of primary GECs derived from *Gkn2*$^{-/-}$ and WT mice in a *H. pylori* SS1 coculture assay (Supplemental Figure 7A). Primary GEC cultures were prepared using established methods (29). Purity of the epithelial cultures was confirmed by staining for pan-cytokeratin and absence of CD45 (immunocytes) and smooth muscle actin (mesenchymal cells). The presence of (GKN2-secreting) SMCs was verified by staining for GKN2 or β-gal in WT and *Gkn2*$^{-/-}$ cultures, respectively (Supplemental Figure 7B). Unstimulated *Gkn2*$^{-/-}$ and WT GECs showed no differences in secretion of 23 chemokines/cytokines at baseline, and, while GECs coincubated with live *H. pylori* for 24 hours showed increased production of CCL3, CCL4, IL-1α, IL-1β, TNF-α, IL-6, and IL-10, these outputs were similar in *Gkn2*$^{-/-}$ and WT cultures (Supplemental Figure 7C). Therefore, the proinflammatory phenotype of *Gkn2*$^{-/-}$ mice is unrelated to chemokine secretion by GECs.

Gkn2$^{-/-}$ *mice show heightened mucosal innate immunity and impaired myeloid-derived suppressor cell responses.* To elucidate mechanisms initiating Th1 inflammatory responses in *Gkn2*$^{-/-}$ mice, we examined the early phase of immune activation at 7 days

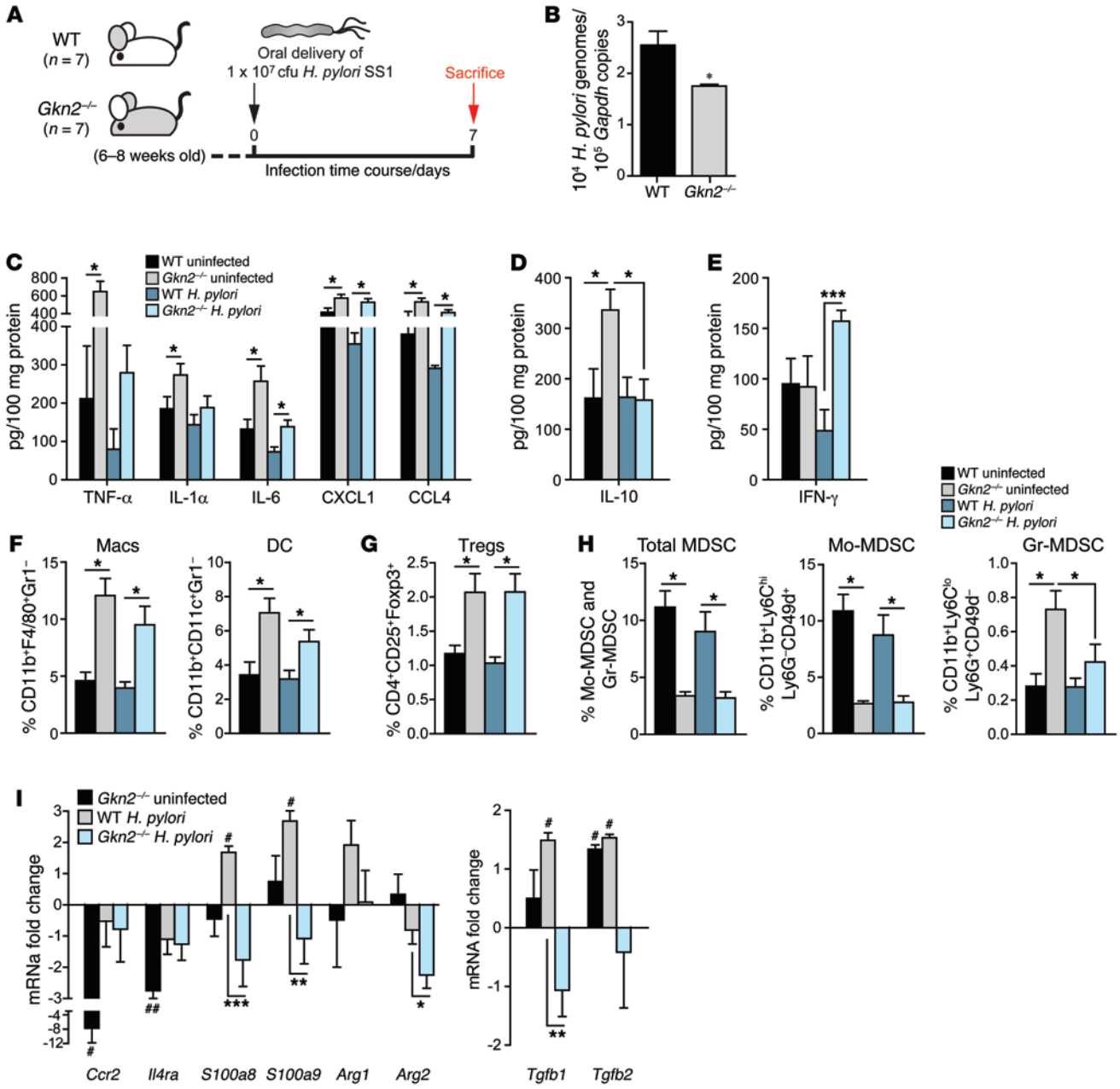

Figure 9. Analysis of gastric mucosal cytokines and immune cell populations in *Gkn2*$^{-/-}$ mice after 7-day *H. pylori* infection. (**A**) Strategy used for 7-day *H. pylori* SS1 infections. (**B**) Q-PCR analysis of *H. pylori* SS1 colonization levels in 7-day infected *Gkn2*$^{-/-}$ and WT stomachs (n = 7 per group). Histograms show mean colonization level (10^4 *H. pylori* genomes per 10^5 *Gapdh* copies). (**C**–**E**) Luminex array analysis of cytokine/chemokine protein levels in corpus homogenates from 7-day infected *Gkn2*$^{-/-}$ and WT (n = 7 per group) and uninfected control mice (n = 8 per group): (**C**) TNF-α, IL-1α, IL-6, CXCL1, and CCL4; (**D**) IL-10; and (**E**) IFN-γ. Histograms show mean normalized levels (pg cytokine/100 mg total protein). (**F**–**H**) Flow cytometry analysis of myeloid/lymphoid cells in stomachs of 7-day infected *Gkn2*$^{-/-}$ mice and uninfected controls (n = 5 per group): (**F**) macrophage (CD11b$^+$F4/80$^+$Gr1$^-$) and DC (CD11c$^+$); (**G**) Treg (CD4$^+$CD25$^+$Foxp3$^+$); and (**H**) total MDSC, monocytic MDSC (Mo-MDSC) (CD11b$^+$Ly6C^{hi}Ly6G$^-$CD49d$^+$), and granulocytic MDSC (Gr-MDSC) (CD11b$^+$Ly6C^{lo} Ly6G$^+$CD49d$^-$) subsets. Histograms show mean cellular prevalence (percentage of total gastric leukocytes). (**I**) QRT-PCR expression profiles of MDSC differentiation (*Ccr2*, *Il4ra*) and activation (*S100a8*, *S100a9*, *Arg1*, *Arg2*, *Tgfb1*, *Tgfb2*) genes in 7-day infected *Gkn2*$^{-/-}$ mice. Error bars represent mean ± SEM. P values were determined using a 2-tailed Student's t test or 2-tailed Mann Whitney U test (**I**, only). Statistical significance compared with WT uninfected control mice: $^{\#}P < 0.05$; $^{\#\#}P < 0.01$. Statistical significance between treatment groups: $^{*}P < 0.05$; $^{**}P < 0.01$; $^{***}P < 0.001$.

after infection with *H. pylori* (ref. 30 and Figure 9A). *H. pylori* colonization levels were again reduced in *Gkn2*$^{-/-}$ mice infected for 7 days (Figure 9B and Supplemental Figure 8) in the absence of evident inflammation. Therefore, the *Gkn2*$^{-/-}$ gastric niche appears less receptive, even to acute *H. pylori* colonization, suggesting that decreased bacterial density occurs prior to the establishment of overt gastritis. To exclude impaired bacterial adhesion to GECs as a mechanism of decreased colonization, we quantified the adhesion of live *H. pylori* to MKN28 GECs transfected with inducible GKN2 expression constructs (Supplemental Methods) and found

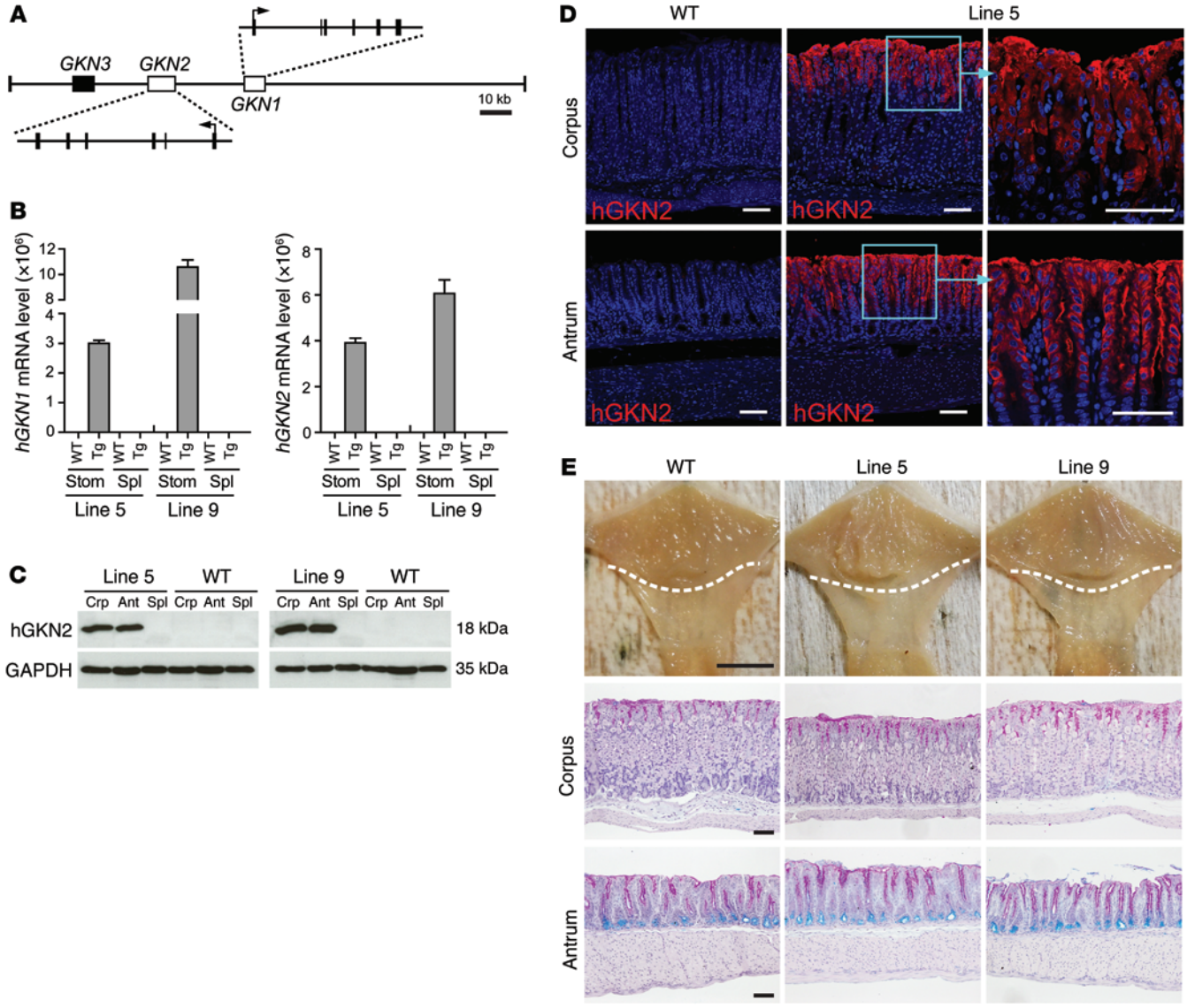

Figure 10. Generation of human *GKN2*/*GKN1*-overexpressing BAC transgenic mice. (**A**) Structure of the 152-kb human BAC transgene showing relative locations of the GKN1 and GKN2 genes (white boxes), with their transcriptional orientation shown in expanded images. The nonexpressed *GKN3* pseudogene is shown as a solid black box. (**B**) QRT-PCR analysis of human *GKN1* (*hGKN1*) and *GKN2* mRNA expression in stomach (Stom) and spleen (Spl) tissues from line 5 and line 9 BAC^{Tg} and WT littermate control mice (n = 3 per group). (**C**) Immunoblot analysis of human GKN2 protein in gastric corpus (Crp), antrum (Ant), and spleen (Spl) tissues of line 5 and line 9 BAC^{Tg} and WT littermate control mice. Protein molecular weights (kDa) are shown. (**D**) Immunofluorescent localization of human GKN2 protein in gastric corpus and antrum of line 5 BAC^{Tg} and WT littermate control mice. Sections were counterstained with DAPI. Scale bar: 50 μm. (**E**) Corpus and antrum mucosal histopathology in line 5 and line 9 BAC^{Tg} mice. Scale bar: 5 mm (macrophotographs); 50 μm (histological images).

that *H. pylori* adhesion was not regulated by GKN2 (Supplemental Figure 9). To characterize immune profiles associated with this host response, we assessed cytokine levels in stomachs of uninfected mice and mice infected for 7 days by luminex array analysis (Supplemental Methods). TNF-α, IL-6, IL-1α, CXCL1, and CCL4 were elevated specifically in corpus (but not antrum) tissues of uninfected *Gkn2*$^{-/-}$ mice, showing no additional increase at 7 days after *H. pylori* infection (Figure 9C and Supplemental Figure 10). *Gkn2*$^{-/-}$ mice also had basally increased IL-10, which decreased to WT levels at 7 days after infection (Figure 9D), concomitant with increased production of IFN-γ (Figure 9E). These results are consistent with basal immunoregulation (to counteract elevated proinflammatory cytokines), which rapidly breaks down upon *H. pylori* challenge, allowing enhanced priming of Th1 immunity.

We next investigated whether the altered gastric cytokine profile of *Gkn2*$^{-/-}$ mice was due to effects in epithelial or immune cells. To address this question, we isolated gastric epithelial and immune cell populations from stomachs of uninfected WT and *Gkn2*$^{-/-}$ mice by FACS (Supplemental Methods) and analyzed their cytokine expression by QRT-PCR. The results showed that *Il1a*, *Il6*, *Tnfa*, and *Ccl4* mRNA were specifically localized within gastric immune cells, not epithelial cells (Supplemental Figure 11). To identify specific immune cell subsets, we next assessed gastric mucosal myeloid and lymphoid populations by flow cytometry (full

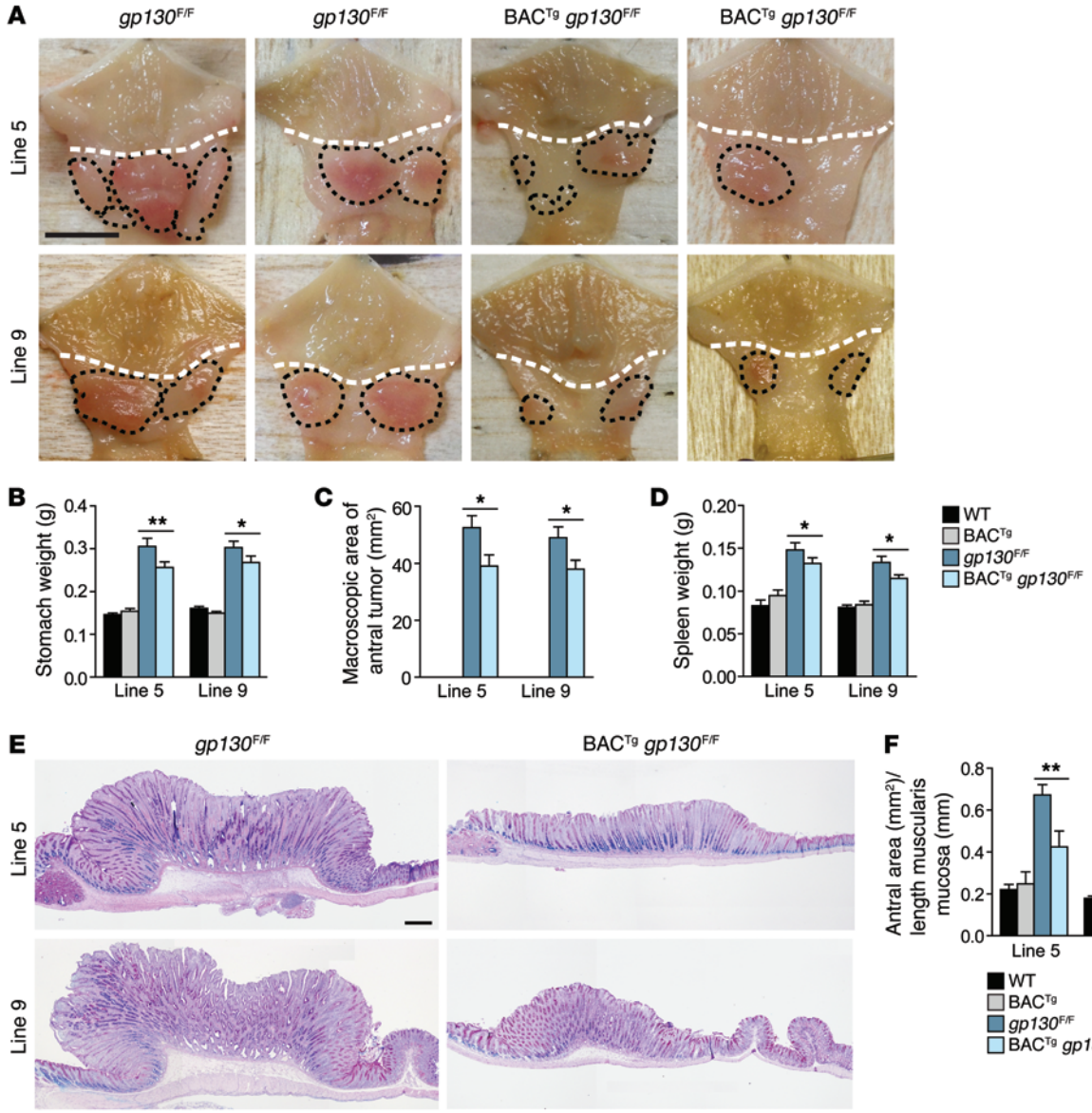

Figure 11. Reduced antral tumor growth in human *GKN2/GKN1*-overexpressing BAC^{Tg} *gp130*$^{F/F}$ mice. (**A**) Representative images of stomachs from line 5 and line 9 BAC^{Tg} *gp130*$^{F/F}$ compound transgenic mice and *gp130*$^{F/F}$ single mutant littermate controls are shown; black dashed lines delineate tumor margins. Scale bar: 5 mm. (**B**) Weight of fresh stomach in grams. (**C**) Macroscopic area of antral tumors in mm^2. (**D**) Weight of fresh spleen in grams in line 5 and line 9 BAC^{Tg} *gp130*$^{F/F}$ compound transgenic (n = 16/n = 16) mice, *gp130*$^{F/F}$ single mutants (n = 12/n = 12), BAC^{Tg} mice (n = 7/n = 14), and WT (n = 5/n = 12) littermate controls. (**E**) Tumor histology in representative BAC^{Tg} *gp130*$^{F/F}$ compound transgenic mice and *gp130*$^{F/F}$ single mutants. Scale bar: 200 μm. (**F**) Morphometric analysis of antral mucosal thickness. Histograms show the mean mucosal thickness as the histological cross section area in mm^2 per unit length of muscularis mucosae. Biological replicates per group as stated for **D**. Error bars represent mean ± SEM. *P* values were determined using a 1-tailed Mann Whitney U test (**B** and **D**) or 1-tailed Student's *t* test (**C** and **F**): $^*P < 0.05$; $^{**}P < 0.01$.

gating strategy shown in Supplemental Figure 12). An increased prevalence of CD11b$^+$F4/80$^+$Gr1$^-$ macrophages and CD11c$^+$ DCs was found in *Gkn2*$^{-/-}$ mice compared with that in WT mice (Figure 9F and Supplemental Figure 13), suggesting that tissue-resident APCs might play a role in shaping the temporal onset, magnitude, and specific polarity of inflammatory responses in *Gkn2*$^{-/-}$ mice.

Induction of immune tolerance to *H. pylori* via recruitment of CD4$^+$CD25$^+$Foxp3$^+$ Tregs occurs during the initial phases of infection, leading to delayed onset of inflammatory pathology (31). We hypothesized that accelerated onset and severity of gastritis in infected *Gkn2*$^{-/-}$ mice could be due to APC-mediated skewing away from a tolerogenic Treg response toward a proinflammatory Th1 response. However, in fact, uninfected *Gkn2*$^{-/-}$ mice had a higher gastric mucosal prevalence of CD4$^+$CD25$^+$Foxp3$^+$ Tregs, which was sustained in mice infected for 7 days (Figure 9G). Therefore, the proinflammatory phenotype of *Gkn2*$^{-/-}$ mice is independent of gastric Treg responses.

Myeloid-derived suppressor cells (MDSCs) are a mixed population of immature myeloid lineages, including granulocyte, macrophage, and DC progenitors (27). MDSCs dampen proinflamma-

tory T cell responses (including Th1 immunity against *H. pylori*; ref. 32) via production of arginase, inducible nitric oxide synthase, and immunosuppressive cytokines (27). In mice, monocytic and granulocytic MDSC subsets can be discriminated by $CD11b^+Ly6C^{hi}Ly6G^-CD49d^+$ and $CD11b^+Ly6C^{lo}Ly6G^+CD49d^-$ surface phenotypes, respectively (33). We assessed MDSCs in stomachs of uninfected *Gkn2*$^{-/-}$ mice and *Gkn2*$^{-/-}$ mice infected for 7 days by flow cytometry. The total number of MDSCs was significantly reduced in uninfected *Gkn2*$^{-/-}$ mice, due to specific deficiency in the monocytic MDSC subset (Figure 9H and Supplemental Figure 13), an effect that was sustained after *H. pylori* infection. These data were corroborated by reduced gastric mRNA expression of the MDSC markers *Ccr2* and *IL4ra* (33) in uninfected *Gkn2*$^{-/-}$ stomachs compared with WT stomachs (Figure 9I). We surmised that enhanced inflammatory responses in *Gkn2*$^{-/-}$ mice could therefore be linked to compromised MDSC responses. Consistent with this expectation, markers of MDSC activation and expansion, *S100a8* and *S100a9*, were upregulated in WT stomachs infected for 7 days but conversely were downregulated in infected *Gkn2*$^{-/-}$ stomachs. Similarly, arginase genes (*Arg1* and *Arg2*) and immunosuppressive cytokines (*Tgfb1* and *Tgfb2*) were upregulated (or trended toward increased expression) in WT stomachs infected for 7 days but were either unchanged or downregulated in infected *Gkn2*$^{-/-}$ stomachs (Figure 9I). These data suggest that impaired activation of MDSCs and breakdown of IL-10–mediated immunoregulation, combined with reciprocal enrichment of APCs (macrophages and DCs), contribute to an enhanced Th1 response in *H. pylori*–infected *Gkn2*$^{-/-}$ mice.

Overexpression of human GKNs restrains gastric tumor growth in vivo. Having established that GKN2 loss can promote GC pathogenesis, we asked whether restoration of GKN2 expression in vivo might suppress disease progression. We reasoned that because GKN2 is normally expressed at unusually high levels, in a discrete and lineage-restricted manner, clinically meaningful outcomes might only be achieved if overexpression to restore GKN2 is driven at a sufficiently high level and in the appropriate cellular context, i.e., specifically in gastric SMCs. We addressed this problem by engineering a large (152-kb) BAC transgene encompassing the entire human *GKN2* and *GKN1* genomic region (Figure 10A). This strategy, resulting in combined human GKN2 and GKN1 expression, was necessary to include sufficient flanking sequence (i.e., containing all native regulatory elements) to drive an amplitude and lineage specificity of overexpression that cannot be accomplished using conventional transgenic approaches. Two BAC transgenic (BAC^{Tg}) founder lines with a high level of transgene expression, line 5 and line 9, were identified by QRT-PCR and immunoblotting studies (Figure 10, B and C). As surmised above, the BAC transgene directed human GKN2 (and GKN1) mRNA/protein expression exclusively to the stomach, with absolute specificity to gastric SMCs (Figure 10D), thus replicating their endogenous expression. BAC^{Tg} mice displayed normal gastric mucosal histology at 12 weeks of age (Figure 10E), showing that overexpression of human GKNs does not alter basal gastric homeostasis. To investigate the impact of human GKN overexpression on gastric tumorigenesis, we generated two independent BAC^{Tg} *gp130*$^{F/F}$ compound mutant strains using BAC^{Tg} mice from line 5 and line 9, respectively. Representative stomachs collected from both BAC^{Tg} *gp130*$^{F/F}$ compound mutant strains are shown in Figure 11A. Antral tumor growth was significantly reduced in 12-week-old BAC^{Tg} *gp130*$^{F/F}$ compound mutants, as assessed by reduced total stomach weight (Figure 11B) and macroscopic area of the tumor mass (Figure 11C) compared with *gp130*$^{F/F}$ single mutant control mice. Interestingly, the splenomegaly that is typically observed in *gp130*$^{F/F}$ mice was significantly reduced in BAC^{Tg} *gp130*$^{F/F}$ compound mutants, consistent with an effect of the reduced tumor load on systemic immunity (Figure 11D). Reduced tumor mass in BAC^{Tg} *gp130*$^{F/F}$ mice was particularly evident in histological analysis, with both compound transgenic lines showing decreased overall thickness of the antral mucosa compared with *gp130*$^{F/F}$ single mutants (Figure 11, E and F). These results establish restoration of human GKNs as a potential therapeutic approach to suppress gastric tumor growth.

Discussion

In a knockout mouse model, we have demonstrated an unexpected antiinflammatory function for the gastric mucus cell–associated protein, GKN2 (8). We have presented in vivo evidence that GKN2 loss, in the context of chronic inflammation induced by *H. pylori* infection, or cytokine-directed tumorigenesis plays a causal role in GC progression. Using a transgenic approach, we have additionally shown that dual overexpression of GKN2 and GKN1 can significantly restrain gastric tumor growth in vivo. This study provides the first major in vivo functional analysis of any of the GKN family proteins to our knowledge. The findings highlight the potential clinical application of these epithelial-derived secreted factors to subdue gastric inflammation and consequent malignant progression.

GKN2 was first linked to GC more than a decade ago, following its initial discovery as a protein downregulated in gastric adenocarcinomas (8, 34). Subsequent studies have shown GKN2 expression loss to be one of the most frequent alterations in both adenocarcinomas (6, 13, 35, 36) and gastric tumor cell lines (6, 35), while, conversely, GKN2 overexpression inhibits proliferation, migration, and invasion of cell lines and tumor xenografts (8, 34, 35). GKN2 therefore appeared to satisfy several of the requisite criteria of a TSG, ostensibly being expressed in normal cell lineages (GECs) giving rise to cancer, imposing restraint on proliferation, and showing absence from tumor cells. Nevertheless, for a genuine TSG function to be formally ascribed, a causal link between expression loss/protein inactivation in a tumor progenitor cell and subsequent oncogenic transformation of derived lineages must be unequivocally established. We instead found that GKN2 loss, in isolation from oncogenic or inflammatory drivers, is insufficient for cell-autonomous transformation, since *Gkn2*$^{-/-}$ mice lacked spontaneous tumor growth or significant epithelial hyperplasia, even at advanced (>30 weeks) age.

Previous studies have focused exclusively on a putative and, now debatable, "classical TSG" function for GKN2 (reviewed in ref. 6) but have not considered alternative roles. Our findings here reveal previously undescribed antiinflammatory and mucosal homeostatic activities as the principal in vivo functions of GKN2. Effects of GKN2 deficiency were relatively mild at baseline, characterized mainly by impaired gastric epithelial differentiation. However, loss of GKN2 was found to profoundly exacerbate gastric immunopathology when placed in context of an inflammatory challenge, namely *H. pylori* infection or genetically induced

hyperactivation of oncogenic gp130/STAT3 signaling. Interestingly, *Gkn2*$^{+/-}$ heterozygous mice (not described in Results section), though phenotypically normal at baseline (Supplemental Figure 14), showed increased susceptibility to *H. pylori*–dependent immunopathology, which is of intermediate severity to that displayed by WT and *Gkn2*$^{-/-}$ mice (Supplemental Figure 15). These data argue that even partial loss of GKN2, as typically seen from the onset of premalignant disease, may be clinically significant.

Genetic loss of GKN2 in *gp130*$^{F/F}$ mice elicited rapid tumorigenesis of the corpus mucosa but, interestingly, did not alter antral tumor growth. However, GKN2 expression is already substantially reduced in *gp130*$^{F/F}$ antral tumors, such that loss of the residual expression in *Gkn2*$^{-/-}$ *gp130*$^{F/F}$ mice would have had little additional impact on tumor growth. As such, these contrasting effects of GKN2 deficiency in corpus and antrum likely relate to the preexisting *gp130*$^{F/F}$ antral pathology and should not necessarily be taken as evidence of preferential GKN2 activity in the corpus. Indeed, our BAC transgenic studies suggest that GKN2 has similar antitumor activity in antral mucosa. Our dual GKN1/GKN2 transgenic strategy has not allowed explicit attribution of the tumor inhibition to GKN2. However, the clear dosage effects of GKN2 shown here (Supplemental Figure 15) argue that transgenic excess of GKN2 would have likely contributed to the reduced tumor load in some manner. It is noteworthy that GKN1 and GKN2 display identical expression in normal gastric SMCs and show coordinate expression loss in GC (7). As such, our tumor rescue data affirm the translational rationale for combined GKN1/GKN2 overexpression in GC. Additionally, these studies provide functional validation for earlier clinical associations of higher level GKN1/GKN2 expression and better outcome in human GC (37).

Strikingly, corpus and antral tumors induced in *Gkn2*$^{-/-}$ *gp130*$^{F/F}$ mice lacked expression of the *Gkn2-lacZ* reporter allele, yet regions of adjacent nontumoral mucosa retained reporter expression. These observations could suggest inactivation of GKN2 within a tumor progenitor cell but are equally consistent with expansion of tumors from immature epithelial lineages lacking GKN2 expression. Long-lived gastric epithelial progenitor cells and bone marrow–derived cells, neither of which express GKN2, have been implicated in the origin of GC (37, 38). Evidence also exists to support transdifferentiation of mitotically quiescent zymogenic cells (zymogenic cell) into a metaplastic lineage that ultimately gives rise to GC (39). On the other hand, the current literature does not support an origin of GC from short-lived gastric SMCs, the sole GKN2-expressing gastric lineage. We therefore propose that GKN2 may not be "inactivated" in a tumor progenitor but rather that the epithelial progenitors to GC have never expressed GKN2, thereby explaining its absence in gastric tumors. Accordingly, GKN2 may instead act non–cell autonomously as an antiinflammatory paracrine signal that maintains homeostatic epithelial turnover and prevents malignant transformation.

Our finding of accelerated immunopathology in *H. pylori*–infected *Gkn2*$^{-/-}$ mice supports an antiinflammatory role for GKN2. Infected *Gkn2*$^{-/-}$ mice showed enhanced mucosal Th1 responses, as evidenced by markedly elevated *Ifng* and *Tbet* mRNA, concomitant skewing toward the IgG2c subclass in the *H. pylori* antibody humoral response, and reduced *H. pylori* colonization. IFN-γ is a key determinant of *H. pylori*–related pathology; *H. pylori*–infected *Ifng*$^{-/-}$ mice do not develop gastritis (40), while transgenic overexpression of IFN-γ is sufficient for induction of atrophic gastritis and metaplasia independently of *H. pylori* infection (41). Thus, elevated IFN-γ is likely central to the premalignant phenotype of infected *Gkn2*$^{-/-}$ mice, especially given that Th17 cytokines were not differentially induced. The localization of immunopathological responses in the corpus in *Gkn2*$^{-/-}$ mice is highly reminiscent of that associated with corpus-predominant gastritis in humans, which is similarly characterized by a Th1-skewed response and carries high risk of progression to advanced metaplasia, dysplasia, and intraepithelial tumor growth (42). Our data indicate that, even partial GKN2 expression loss, particularly in the context of Th1-type cytokine gene polymorphisms (43, 44), may strongly influence premalignant outcomes in *H. pylori*–infected individuals with corpus-predominant disease.

In short-term (7-day) infection studies, we found that Th1 immune bias in *Gkn2*$^{-/-}$ mice may relate to heightened basal innate immunity. *Gkn2*$^{-/-}$ mice showed mucosal enrichment of proinflammatory cytokines and increased prevalence of macrophages and DCs, which likely prime an exaggerated IFN-γ response upon exposure to *H. pylori*. Both macrophages and DCs, via professional antigen-presenting capabilities, are known to initiate adaptive responses against *H. pylori*, in part by secretion of Th1-polarizing (and Th17-polarizing) cytokines, IL-12 (and IL-23), respectively (45–48). Basally increased IL-10 (and mucosal Tregs) may also explain why *Gkn2*$^{-/-}$ mice resist pathological progression when unchallenged. Another factor contributing to the *Gkn2*$^{-/-}$ phenotype may have been MDSCs, which inhibit T cell proliferation in mouse models of GC (19) and suppress effector T cells, which drive gastric immunopathology (49, 50). Impaired gastric MDSC responses to *H. pylori* infection may have contributed to the accelerated T cell–driven immunopathology in this model. Although MDSCs have been widely described to exacerbate cancer progression via suppression of CD8$^+$ T cell–mediated antitumor immunity and promotion of angiogenesis (27), recent work suggests that MDSCs, via secretion of IL-10, may also participate in the resolution of bacterial inflammation (51). Proinflammatory roles of MDSCs in established *H. pylori* infections have been proposed by others (32, 52). Our data argue that immunosuppressive functions of MDSCs are required to dampen early gastric responses to *H. pylori* infection. Given that gastric SMCs are the sole physiological source of GKN2 (see Figure 1D; Figure 2, D–N; refs. 6, 9, and literature cited therein), it is reasonable to argue that altered gastric mucosal immune profiles of *Gkn2*$^{-/-}$ mice relate to paracrine deficiency of secreted GKN2 protein. Understanding the molecular basis of GKN2 paracrine activity toward specific myeloid cell subsets, including MDSCs, will be a priority if its clinical potential is to be realized.

Functional effects of GKN2 loss have been firmly established here, yet a key question not addressed by this study is what triggers GKN2 loss (or decreased expression) in the first place? Neither cytogenetic aberrations encompassing chromosome 2p13.3 (where the GKNs are located) nor *GKN2* somatic mutations have been reported in GC (53–55), while epigenetic silencing of *GKN2* applies to only a minority of gastric tumors (55). Together, these studies argue that mechanisms other than cytogenetic or epigenetic anomalies are mainly responsible for GKN2 expression loss. Our findings of decreased *Gkn2* mRNA in *Il1b* and *Gm-CSf*

transgenic overexpressing mice or following IL-11/gp130/STAT3 hyperactivation (see Figure 1F) suggest a mechanism of negative transcriptional regulation via proinflammatory cytokine signaling. This is corroborated by earlier work showing transcriptional repression of a *GKN2* promoter-reporter construct induced by exogenous IL-1β, IL-6, and TNF-α treatment or NF-κB cotransfection in cultured GECs (56). The appropriate expression dosage of GKN2 protein (and associated antiinflammatory activity) may therefore be governed by promoter *cis* elements, functioning collectively as a cytokine-responsive "transcriptional rheostat." Such a mechanism could explain the progressive loss of GKN2, in concert with worsening inflammation, as well as the recovery of GKN2 expression after *H. pylori* eradication and restoration of mucosal homeostasis (12).

In summary, we demonstrate an antiinflammatory role for the gastric epithelial-secreted protein, GKN2. We provide the first in vivo functional evidence to our knowledge that loss of GKN2 expression, leading to deregulated Th1 immunity and exacerbation of inflammatory pathology, plays a causal role in GC progression. Critically, we have also shown that restoration of human GKN expression can interrupt gastric tumor growth in vivo. Current preventative therapy for GC is based on antibiotic eradication of *H. pylori* (57). Our findings suggest complementation of GKN2 function as an alternative disease management strategy, particularly in the approximately 20% of infected individuals for whom antibiotic treatment fails (57) or in those presenting with irreversible premalignant disease (58).

Methods

Human tissues. *H. pylori*–infected and disease-free human gastric epithelial tissues, GCs, and premalignant "adjacent-to-cancer" tissues with intestinal metaplasia were obtained endoscopically (59, 60).

Gene targeting. Embryonic stem cell clones (C57BL/6NTac genetic background) carrying a VelociGene *lacZ* reporter/loxP-flanked neomycin selection cassette (61) at the *Gkn2* locus were purchased from the Knockout Mouse Project repository (https://www.komp.org/). Injection of targeted embryonic stem cell clones into BALB/c recipient blastocysts and backcrossing (C57BL/6) of resulting chimeric mice to generate $Gkn2^{+/-}$ mice was performed at the Australian Phenomics Network laboratories, Monash, Clayton, Victoria, Australia (http://www.australianphenomics.org.au/).

Generation of BAC transgenic mice. A 152-kb DNA fragment containing the human *GKN1* and *GKN2* genomic region was excised from a BAC clone (RP11-H2112) by *Not*I digestion and then purified from the vector backbone by pulsed field gel electrophoresis through a 1% agarose, Tris/borate/EDTA gel. Purified BAC DNA was subjected to tube dialysis against 500 volumes TE buffer (10 mM Tris, 1 mM EDTA) overnight at 4°C, followed by microdialysis on 0.05-μm filters (Millipore) against 100 volumes microinjection buffer (10 mM Tris-HCl, pH 7.5, 100 mM NaCl, 0.1 mM EDTA, 30 μM spermine, 70 μM spermidine) overnight at 4°C. Dialyzed BAC DNA was diluted to a concentration 0.5 ng/μl and then used for microinjection into C57BL/6J × DBA/2J F2 hybrid zygotes. BAC^{Tg} founder animals were identified by PCR and Southern blotting analysis. Two founder lines (lines 5 and 9) with high-level expression of human GKNs were selected and backcrossed to the C57BL/6 strain for 6 generations prior to commencement of experiments. To generate BAC^{Tg} $gp130^{F/F}$ compound transgenic mice, BAC^{Tg} line 5 and BAC^{Tg} line 9 mice (C57BL/6) were each independently crossed with $gp130^{F/F}$ mice (C57BL/6).

Mice. Mouse strains, including the $gp130^{F/F}$ mutant (a gift from Matthias Ernst, Olivia Newton John Cancer Research Institute, Melbourne, Australia; ref. 15), $HK\beta^{-/-}$ (a gift from Ian van Driel, Bio21 Molecular Science and Biotechnology Institute, Melbourne, Australia; ref. 62), *TgCMV-cre1Cgn* transgenic ($CMV\text{-}Cre^{Tg}$; a gift from Ursula Lichtenberg, University of Cologne, Cologne, Germany; ref. 20), $Tff1^{-/-}$ (17), $Gkn2^{-/-}$ (generated in-house), and human *GKN2/GKN1* BAC transgenic mice (generated in-house), were maintained on a C57BL/6 genetic background. All strains were housed under specific pathogen–free conditions. Gastric tissues from *HKβ* promoter *Gm-CSf* transgenic ($Gm\text{-}CSf^{Tg}$) mice (BALB/c strain background) (63) were a gift from Ian van Driel. Gastric tissues were also obtained from *HKβ* promoter *IL1β* transgenic ($IL1\beta^{Tg}$) mice that have been described previously (19). All experiments involving the above strains used matched WT littermate controls.

H. pylori infection in mice. Mouse-adapted *H. pylori* SS1 ($vacA^{+}$, *cag*PAI dysfunctional; ref. 25) was grown in brain-heart infusion broth (Oxoid) containing 5% horse serum (JRH Biosciences) and 0.02% amphostat (Invitrogen), under microaerophilic conditions for 24 hours at 37°C. Mice were infected intragastrically with a single dose of 10^7 *H. pylori* SS1 CFU suspended in 100 μl brain-heart infusion broth as described previously (64). *H. pylori* colonization levels were subsequently quantified by TaqMan quantitative PCR assay on stomach extracts (full details provided in the Supplemental Methods) or by CFU assay as described previously (64).

Histopathology. Stomach tissues were collected at necropsy, fixed in 4% paraformaldehyde in PBS overnight, and processed for standard paraffin wax histology. Slides were stained for presence of neutral (gastric-type) and acidic (intestinal-type) mucins with Alcian blue PAS (AB-PAS) reagent and scored for pathology on a scale of 0 to 4 by a blinded observer as described previously (65), with modifications (full details, including criteria for individual scores, are provided in the Supplemental Methods).

Immunohistochemistry and immunofluorescence. Immunohistochemistry was performed as described previously (9). Bound immunocomplexes were detected using Vectastain ABC reagents (Vector Laboratories), and staining was visualized by incubation in 3, 3′-diaminobenzidine tetrahydrochloride reagent (Sigma-Aldrich). Immunofluorescence in cultured cells was performed as described previously (9). Primary antibodies and lectins used are as follows: rabbit polyclonal anti-mouse GKN2 (R771-B3) and anti-human GKN2 (R779-B3; custom generated, see Supplemental Methods), each diluted 1:500; mouse monoclonal anti-human Ki67 (Abcam) diluted 1:500; lectin *GS*-II from *Griffonia simplicifolia* (EY Labs) used at 10 μg/ml; sheep polyclonal anti-human pepsinogen II (Abcam) diluted 1:100; mouse monoclonal anti–H^+K^+ ATPase β subunit (Abcam, ab2866) diluted 1:2,000; rabbit polyclonal anti-TFF1 and TFF2 (custom generated) (60) diluted 1:750 and 1:1,000, respectively; mouse monoclonal anti-MUC5AC-biotin conjugate (Abcam, ab79082) diluted 1:400; rabbit monoclonal anti-CDX2-Alexa Fluor 488 conjugate (Abcam, ab195007) diluted 1:200; and chicken polyclonal anti-β-gal (Abcam, ab9361) diluted 1:200. Immunofluorescent detection of bound primary antibodies was achieved using the following secondary antibody conjugates: donkey anti-rabbit IgG-Alexa Fluor 594, goat-anti mouse IgG Alexa Fluor 488, streptavidin-Alexa Fluor 488, streptavidin-Alexa Fluor 568, and anti-sheep IgG Alexa Fluor 594 (all from Invitrogen

Molecular Probes) and goat anti-chicken IgY-DyLight 488 (Abcam, ab96947). Samples were mounted in Pro-Long Gold medium containing DAPI counterstain (Invitrogen). Fluorescence images were captured using a Zeiss LSM 780 laser scanning confocal microscope and processed using ZEN software (Zeiss).

Flow cytometry. Cell suspensions were prepared from whole stomach tissue using Gentle MACS lamina propria dissociation reagents and protocols (Miltenyi Biotech). Total leukocytes were purified from cell suspensions by Percoll (GE Healthcare) density gradient centrifugation (40%/80% Percoll interface) and then resuspended in 2% FBS, 2 mM EDTA in HBSS. Purified leukocytes were stained for presence of surface markers specific to macrophages, DCs, and MDSCs using the following anti-mouse monoclonal antibodies: CD11b (Brilliant Violet 421 101235 [1:1,000]; PE 557397 [1:500]), CD49d (FITC, 103605 [1:1,000]), Gr1 (PerCP-Cy5.5, 552093 [1:1,000]), Ly6C (PerCP, 128028 [1:1,000]), F4/80 (Alexa Fluor 700, 123130 [1:1,000]), Ly6G (APC/Cy7, 127624 [1:500]), and CD45 (V500, 561487 [1:500]) (all Biolegend) and CD11c (APC, 17-0114-82 [1:1,000]) (eBioscience). Tregs were detected using the Mouse Regulatory T Cell Staining Kit (eBioscience, 88-8111-40): CD4 (FITC [1:500]), CD25 (APC [1:500]), and Foxp3 (PE [1:200]). CountBright absolute counting beads (Molecular Probes) were used to determine total cell number per sample. Cell viability was assessed by propidium iodide dye exclusion. Leukocytes were gated based on forward and side scatter properties, with subsequent gating on specific myeloid cell markers as described above (gating strategies are shown in Supplemental Figure 12). Data collection was performed on a BD LSR II Flow Cytometer, and analysis was performed using FACSDiva software (both BD Biosciences).

Gene expression. QRT-PCR was performed as described previously (66). Primer sequences were designed using the primer3 tool (http://frodo.wi.mit.edu/primer3/) and are listed together with cycling parameters in the Supplemental Methods. Relative gene expression was normalized to expression of internal reference gene *GAPDH* (human) or *Rpl32* (mouse) using the $-2\Delta\Delta$Ct method, where $-2\Delta\Delta Ct = \Delta Ct$ sample $- \Delta Ct$ calibrator (67).

Statistics. Data were analyzed with GraphPad Prism V5.1 software. Data are presented as the mean ± SEM. Statistical analysis was performed by 1-way analysis of variance, with 2-group comparisons tested post hoc, using a 1- or 2-tailed Student's *t* test for parametric data or a Mann-Whitney *U* test for nonparametric data. *P* values of 0.05 or lower were considered statistically significant.

Study approval. Mouse experiments were approved by the Murdoch Children's Research Institute Animal Ethics Committee (approval no. A693, A700, and A713). Approval for experiments on human tissues was obtained from the Royal Melbourne Hospital Human Research Ethics Committee (approval no. 2004.176) and the Kanazawa University Ethics Committee for Human Genome Research (approval no. 174.2008). Written informed consent was obtained for all study participants.

Author contributions

TRM and LOC performed most of the experiments and data analysis. YTC, MS, LMJ, JD, BNR, GZN, SJ, AC, DEO, BK, and SM contributed to experiments. LMJ, JD, and MS contributed to data analysis. JGF, TCW, TM, and RLF contributed reagents, materials, or protocols. TRM, PS, LMJ, and ASG conceived of, designed, and led the study. TRM wrote the manuscript. TRM, PS, LMJ, ASG, JD, TM, and RLF edited/revised the manuscript.

Acknowledgments

We thank the Australian Phenomics Network for assistance with generation of *Gkn2*$^{-/-}$ mice and Elizabeth Williams for pronuclear injections of BAC DNA and generation of transgenic mice at the Transgenic Animal Service of Queensland, University of Queensland, St. Lucia, Australia. We thank Matthew Burton, the Flow Cytometry and Imaging Facility, Murdoch Children's Research Institute, for advice and assistance with flow cytometry analysis. This study was supported by a project grant (1047208) from the National Health and Medical Research Council (NHMRC); research fellowships awarded to T.R. Menheniott (1026674), A.S. Giraud (607330), L.M. Judd (1008776) and P. Sutton (1020387) by the NHMRC; a fellowship (DFG DA1161/5-1) awarded to J. Däbritz by the German Research Foundation; and the Victorian Government's Medical Research Operational Infrastructure Support Program.

Address correspondence to: Trevelyan R. Menheniott, Murdoch Children's Research Institute, The Royal Children's Hospital, 50 Flemington Road, Parkville, Victoria, 3052, Australia. Phone: 61.3.9936.6265; E-mail: treve.menheniott@mcri.edu.au.

1. Ferlay J, et al. Cancer incidence and mortality worldwide: sources, methods and major patterns in GLOBOCAN 2012. *Int J Cancer*. 2015;136(5):E359–E386.
2. Correa P, Haenszel W, Cuello C, Tannenbaum S, Archer M. A model for gastric cancer epidemiology. *Lancet*. 1975;2(7924):58–60.
3. Schier S, Wright NA. Stem cell relationships and the origin of gastrointestinal cancer. *Oncology*. 2005;69(suppl 1):9–13.
4. Hoffmann W. Self-renewal of the gastric epithelium from stem and progenitor cells. *Front Biosci (Schol Ed)*. 2013;5:720–731.
5. Hedlund J, Johansson J, Persson B. BRICHOS – a superfamily of multidomain proteins with diverse functions. *BMC Res Notes*. 2009;2:180.
6. Menheniott TR, Kurklu B, Giraud AS. Gastrokines: stomach-specific proteins with putative homeostatic and tumor suppressor roles. *Am J Physiol Gastrointest Liver Physiol*. 2013;304(2):G109–G121.
7. Martin TE, et al. A novel mitogenic protein that is highly expressed in cells of the gastric antrum mucosa. *Am J Physiol Gastrointest Liver Physiol*. 2003;285(2):G332–G343.
8. Du JJ, et al. [Down-regulated full-length novel gene GDDR and its effect on gastric cancer]. *Zhonghua Yi Xue Za Zhi*. 2003;83(13):1166–1168.
9. Menheniott TR, et al. A novel gastrokine, Gkn3, marks gastric atrophy and shows evidence of adaptive gene loss in humans. *Gastroenterology*. 2010;138(5):1823–1835.
10. Geahlen JH, et al. Evolution of the human gastrokine locus and confounding factors regarding the pseudogenicity of GKN3. *Physiol Genomics*. 2013;45(15):667–683.
11. Oien KA, et al. Gastrokine 1 is abundantly and specifically expressed in superficial gastric epithelium, down-regulated in gastric carcinoma, and shows high evolutionary conservation. *J Pathol*. 2004;203(3):789–797.
12. Resnick MB, et al. Global analysis of the human gastric epithelial transcriptome altered by Helicobacter pylori eradication in vivo. *Gut*. 2006;55(12):1717–1724.
13. May FE, Griffin SM, Westley BR. The trefoil factor interacting protein TFIZ1 binds the trefoil protein TFF1 preferentially in normal gastric mucosal cells but the co-expression of these proteins is deregulated in gastric cancer. *Int J Biochem Cell Biol*. 2009;41(3):632–640.
14. Westley BR, Griffin SM, May FE. Interaction between TFF1, a gastric tumor suppressor trefoil protein, and TFIZ1, a brichos domain-containing protein with homology to SP-C. *Biochemistry*. 2005;44(22):7967–7975.
15. Tebbutt NC, et al. Reciprocal regulation of gas-

trointestinal homeostasis by SHP2 and STAT-mediated trefoil gene activation in gp130 mutant mice. *Nat Med*. 2002;8(10):1089–1097.
16. Judd LM, et al. Gastric cancer development in mice lacking the SHP2 binding site on the IL-6 family co-receptor gp130. *Gastroenterology*. 2004;126(1):196–207.
17. Lefebvre O, et al. Gastric mucosa abnormalities and tumorigenesis in mice lacking the pS2 trefoil protein. *Science*. 1996;274(5285):259–262.
18. Oshima H, Matsunaga A, Fujimura T, Tsukamoto T, Taketo MM, Oshima M. Carcinogenesis in mouse stomach by simultaneous activation of the Wnt signaling and prostaglandin E2 pathway. *Gastroenterology*. 2006;131(4):1086–1095.
19. Tu S, et al. Overexpression of interleukin-1β induces gastric inflammation and cancer and mobilizes myeloid-derived suppressor cells in mice. *Cancer Cell*. 2008;14(5):408–419.
20. Schwenk F, Baron U, Rajewsky K. A cre-transgenic mouse strain for the ubiquitous deletion of loxP-flanked gene segments including deletion in germ cells. *Nucleic Acids Res*. 1995;23(24):5080–5081.
21. Howlett M, et al. The interleukin-6 family cytokine interleukin-11 regulates homeostatic epithelial cell turnover and promotes gastric tumor development. *Gastroenterology*. 2009;136(3):967–977.
22. Ernst M, et al. STAT3 and STAT1 mediate IL-11-dependent and inflammation-associated gastric tumorigenesis in gp130 receptor mutant mice. *J Clin Invest*. 2008;118(5):1727–1738.
23. Howlett M, et al. Differential regulation of gastric tumor growth by cytokines that signal exclusively through the coreceptor gp130. *Gastroenterology*. 2005;129(3):1005–1018.
24. Correa P, Piazuelo MB. The gastric precancerous cascade. *J Dig Dis*. 2012;13(1):2–9.
25. Lee A, O'Rourke J, De Ungria MC, Robertson B, Daskalopoulos G, Dixon MF. A standardized mouse model of Helicobacter pylori infection: introducing the Sydney strain. *Gastroenterology*. 1997;112(4):1386–1397.
26. Weis VG, Goldenring JR. Current understanding of SPEM and its standing in the preneoplastic process. *Gastric Cancer*. 2009;12(4):189–197.
27. Gabrilovich DI, Nagaraj S. Myeloid-derived suppressor cells as regulators of the immune system. *Nat Rev Immunol*. 2009;9(3):162–174.
28. Peek RM Jr, Fiske C, Wilson KT. Role of innate immunity in Helicobacter pylori-induced gastric malignancy. *Physiol Rev*. 2010;90(3):831–858.
29. Viala J, et al. Nod1 responds to peptidoglycan delivered by the Helicobacter pylori cag pathogenicity island. *Nat Immunol*. 2004;5(11):1166–1174.
30. Thompson LJ, et al. Chronic Helicobacter pylori infection with Sydney strain 1 and a newly identified mouse-adapted strain (Sydney strain 2000) in C57BL/6 and BALB/c mice. *Infect Immun*. 2004;72(8):4668–4679.
31. Kao JY, et al. Helicobacter pylori immune escape is mediated by dendritic cell-induced Treg skewing and Th17 suppression in mice. *Gastroenterology*. 2010;138(3):1046–1054.
32. Zhuang Y, et al. A pro-inflammatory role for Th22 cells in Helicobacter pylori-associated gastritis. *Gut*. 2015;64(9):1368–1378.
33. Talmadge JE, Gabrilovich DI. History of myeloid-derived suppressor cells. *Nat Rev Cancer*. 2013;13(10):739–752.
34. Du JJ, et al. [Study on novel gene GDDR related to gastric cancer]. *Zhonghua Wai Ke Za Zhi*. 2005;43(1):10–13.
35. Dai J, Zhang N, Wang J, Chen M, Chen J. Gastrokine-2 is downregulated in gastric cancer and its restoration suppresses gastric tumorigenesis and cancer metastasis. *Tumour Biol*. 2014;35(5):4199–4207.
36. Moss SF, et al. Decreased expression of gastrokine 1 and the trefoil factor interacting protein TFIZ1/GKN2 in gastric cancer: influence of tumor histology and relationship to prognosis. *Clin Cancer Res*. 2008;14(13):4161–4167.
37. Houghton J, et al. Gastric cancer originating from bone marrow-derived cells. *Science*. 2004;306(5701):1568–1571.
38. Barker N, et al. Lgr5(+ve) stem cells drive self-renewal in the stomach and build long-lived gastric units in vitro. *Cell Stem Cell*. 2010;6(1):25–36.
39. Nam KT, et al. et al. Mature chief cells are cryptic progenitors for metaplasia in the stomach. *Gastroenterology*. 2010;139(6):2028–2037.
40. Smythies LE, Waites KB, Lindsey JR, Harris PR, Ghiara P, Smith PD. Helicobacter pylori-induced mucosal inflammation is Th1 mediated and exacerbated in IL-4, but not IFN-γ, gene-deficient mice. *J Immunol*. 2000;165(2):1022–1029.
41. Syu LJ, et al. Transgenic expression of interferon-gamma in mouse stomach leads to inflammation, metaplasia, and dysplasia. *Am J Pathol*. 2012;181(6):2114–2125.
42. Miehlke S, et al. Severe expression of corpus gastritis is characteristic in gastric cancer patients infected with Helicobacter pylori. *Br J Cancer*. 1998;78(2):263–266.
43. El-Omar EM, et al. Interleukin-1 polymorphisms associated with increased risk of gastric cancer. *Nature*. 2000;404(6776):398–402.
44. Hou L, et al. Polymorphisms in Th1-type cell-mediated response genes and risk of gastric cancer. *Carcinogenesis*. 2007;28(1):118–123.
45. Guiney DG, Hasegawa P, Cole SP. Helicobacter pylori preferentially induces interleukin 12 (IL-12) rather than IL-6 or IL-10 in human dendritic cells. *Infect Immun*. 2003;71(7):4163–4166.
46. Kranzer K, et al. Induction of maturation and cytokine release of human dendritic cells by Helicobacter pylori. *Infect Immun*. 2004;72(8):4416–4423.
47. Mitchell P, et al. Chronic exposure to Helicobacter pylori impairs dendritic cell function and inhibits Th1 development. *Infect Immun*. 2007;75(2):810–819.
48. Khamri W, et al. Helicobacter pylori stimulates dendritic cells to induce interleukin-17 expression from $CD4^+$ T lymphocytes. *Infect Immun*. 2010;78(2):845–853.
49. Stummvoll GH, et al. Th1, Th2, and Th17 effector T cell-induced autoimmune gastritis differs in pathological pattern and in susceptibility to suppression by regulatory T cells. *J Immunol*. 2008;181(3):1908–1916.
50. Quiding-Jarbrink M, Lundin BS, Lonroth H, Svennerholm AM. $CD4^+$ and $CD8^+$ T cell responses in Helicobacter pylori-infected individuals. *Clin Exp Immunol*. 2001;123(1):81–87.
51. Poe SL, et al. STAT1-regulated lung MDSC-like cells produce IL-10 and efferocytose apoptotic neutrophils with relevance in resolution of bacterial pneumonia. *Mucosal immunology*. 2013;6(1):189–199.
52. Ng GZ, et al. The Muc1 mucin protects against Helicobacter pylori pathogenesis in mice by regulation of the NLRP3 inflammasome [published online ahead of print April 8, 2015]. *Gut*. doi:10.1136/gutjnl-2014-307175.
53. Chetty R, Naidoo R, Tarin M, Sitti C. Chromosome 2p, 3p, 5q and 18q status in sporadic gastric cancer. *Pathology*. 2002;34(3):275–281.
54. Panani AD. Cytogenetic and molecular aspects of gastric cancer: clinical implications. *Cancer Lett*. 2008;266(2):99–115.
55. Yoon JH, et al. Inactivation of the Gastrokine 1 gene in gastric adenomas and carcinomas. *J Pathol*. 2011;223(5):618–625.
56. Baus-Loncar M, Lubka M, Pusch CM, Otto WR, Poulsom R, Blin N. Cytokine regulation of the trefoil factor family binding protein GKN2 (GDDR/TFIZ1/blottin) in human gastrointestinal epithelial cells. *Cell Physiol Biochem*. 2007;20(1–4):193–204.
57. Selgrad M, Malfertheiner P. Treatment of Helicobacter pylori. *Curr Opin Gastroenterol*. 2011;27(6):565–570.
58. Genta RM, Rugge M. Gastric precancerous lesions: heading for an international consensus. *Gut*. 1999;45(suppl 1):I5–I8.
59. Jackson CB, et al. Augmented gp130-mediated cytokine signalling accompanies human gastric cancer progression. *J Pathol*. 2007;213(2):140–151.
60. Peterson AJ, et al. Helicobacter pylori infection promotes methylation and silencing of trefoil factor 2, leading to gastric tumor development in mice and humans. *Gastroenterology*. 2010;139(6):2005–2017.
61. Valenzuela DM, et al. High-throughput engineering of the mouse genome coupled with high-resolution expression analysis. *Nat Biotechnol*. 2003;21(6):652–659.
62. Scarff KL, Judd LM, Toh BH, Gleeson PA, Van Driel IR. Gastric H(+),K(+)-adenosine triphosphatase beta subunit is required for normal function, development, and membrane structure of mouse parietal cells. *Gastroenterology*. 1999;117(3):605–618.
63. Biondo M, Nasa Z, Marshall A, Toh BH, Alderuccio F. Local transgenic expression of granulocyte macrophage-colony stimulating factor initiates autoimmunity. *J Immunol*. 2001;166(3):2090–2099.
64. Wee JL, et al. Protease-activated receptor-1 down-regulates the murine inflammatory and humoral response to Helicobacter pylori. *Gastroenterology*. 2010;138(2):573–582.
65. Fox JG, et al. Accelerated progression of gastritis to dysplasia in the pyloric antrum of $TFF2^{-/-}$ C57BL6 × Sv129 Helicobacter pylori-infected mice. *Am J Pathol*. 2007;171(5):1520–1528.
66. Kurklu B, et al. Lineage-specific RUNX3 hypomethylation marks the preneoplastic immune component of gastric cancer. *Oncogene*. 2014;34(22):2856–2866.
67. Livak KJ, Schmittgen TD. Analysis of relative gene expression data using real-time quantitative PCR and the 2(-ΔΔC(T)) Method. *Methods*. 2001;25(4):402–408.